

ORIGINAL CONTRIBUTION

Image Processing Regularization Filters on Layered Architecture

HARUO KOBAYASHI*, TAKASHI MATSUMOTO†, TETSUYA YAGI‡, AND TAKUJI SHIMMI†

*Yokogawa Electric Corporation, †Waseda University, and ‡Kyushu Institute of Technology

(Received 15 November 1991; revised and accepted 24 July 1992)

Abstract—Layered architecture is proposed for solving a class of regularization problems in image processing. There are two major hurdles in the implementation of regularization filters with second or higher order smoothness constraints: (a) **Stability**: With second or higher order constraints, a direct implementation of a regularization filter necessitates negative conductance which, in turn, gives rise to stability problems. (b) **Wiring Complexity**: A direct implementation of an N -th order regularization filter requires wiring between every pair of k -th nearest nodes for all k , $1 \leq k \leq N$. Even though one of the authors managed to layout an $N = 2$ chip, the implementation of an $N \geq 3$ chip would be an extremely difficult, if not impossible, task. The regularization filter architecture proposed here (a) requires no negative conductance; and (b) necessitates wiring only between nearest nodes. Smoothing-Contrast-Enhancement filter is given as an example of application. Since this filter is extremely fast, it will have a natural application to smart sensing, i.e., to the simultaneous achievement of sensing and processing. It is also explained how this architecture has been inspired by physiological findings on lower vertebrate retina by one of the authors.

Keywords—Regularization, Vision chip, Layered architecture, Analog CMOS, Image processing, Smart sensor.

1. INTRODUCTION

1.1. Purpose

The Tikhonov regularization theory solves some of the interesting early vision problems (Poggio, Torre, & Koch, 1985). When implemented on a parallel analog processing chip, regularization filters are endowed with an extremely high processing speed, and orders of magnitude faster than digital signal processors. This is a result of the fact that the processing (computation) is

done by the dynamics induced by the parasitic capacitors of transistors, and the processed image is given as a stable limit point of the dynamics. This naturally indicates an applicability to smart sensors. In other words, in addition to sensing, a chip performs signal processing (see, e.g., Gruss, Carley, & Kanade, 1991).

Most of the early vision chips implemented so far have first order smoothness constraints (Harris, 1988; Harris, Koch, Luo, & Wyatt, 1989; Hutchinson, Koch, Luo, & Mead, 1988; Liu & Harris, 1989; Mathur, Lin, & Wang, 1990; Mead, 1989; Mead & Mahowald, 1988). This seems to be attributable to the fact that first order smoothness constraints can be implemented by a parallel network where (a) each node is connected with only its immediate neighbors; and (b) only passive conductance is required. If one goes beyond the first order smoothness constraints, however, one encounters two major difficulties. In order to be precise, let us look at Figure 1, which shows the architecture of a second order regularization solver (Kobayashi, White, & Abidi 1990, 1991) implemented by one of the authors. It is intended for smoothing out a noisy image in an extremely fast manner ($\leq 5 \mu\text{s}$). Theoretical justification for this came from the important result that the second order regularization filter closely approximates a Gaussian filter (Poggio, Voorhees, & Yuille, 1985). Even though the chip did work successfully (Figure

Acknowledgements: Earlier discussions with M. Kawato of ATR Visual Perception Laboratory were very helpful. Discussions with J. Harris of MIT AI Laboratory greatly enhanced the paper. The constructive comments by the reviewers helped improve the contents. Thanks are also due to Y. Togawa of the Science University of Tokyo, D. Terzopoulos of the University of Toronto, S. Yasui of the Kyushu Institute of Technology, N. Ieda, A. Iwata, Y. Amemiya, K. Uchiyama of NTT VLSI Laboratory, A. Hio, J. Sanekata, K. Tanaka and N. Takaku of Waseda University for discussions. S. Miyake and T. Ito of NHK Visual Perception Laboratory kindly took time to provide us with unpublished details of the work of Yasuda, Yamaguchi, Fukushima, and Nagata, including the real hardware.

Requests for reprints should be sent to T. Matsumoto, Department of Electrical Engineering, Waseda University, 3-4-1 Ohkubo, Shinjuku-ku, Tokyo 169 Japan.

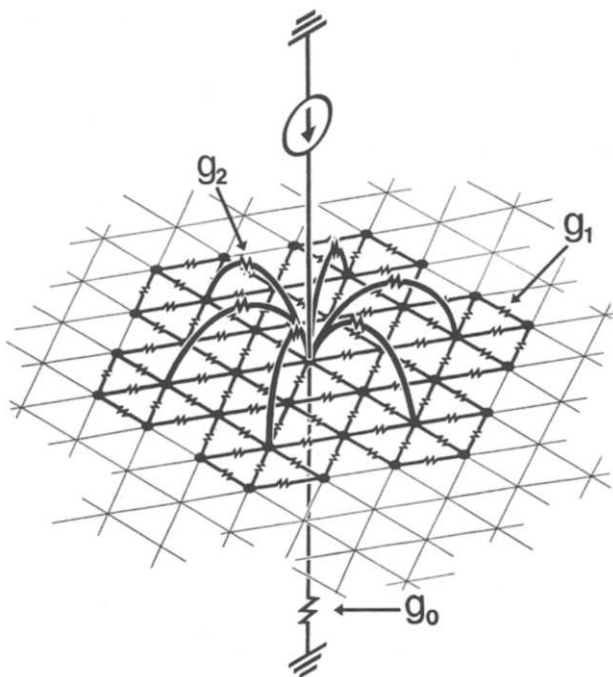


FIGURE 1. Architecture of a 2nd order regularization chip.

2(a) shows a typical measured impulse response, Figure 2(b) shows several smoothed images, Figure 2(c) shows a schematic diagram, and Figure 2(d) shows a chip photograph), two hurdles had to be cleared:

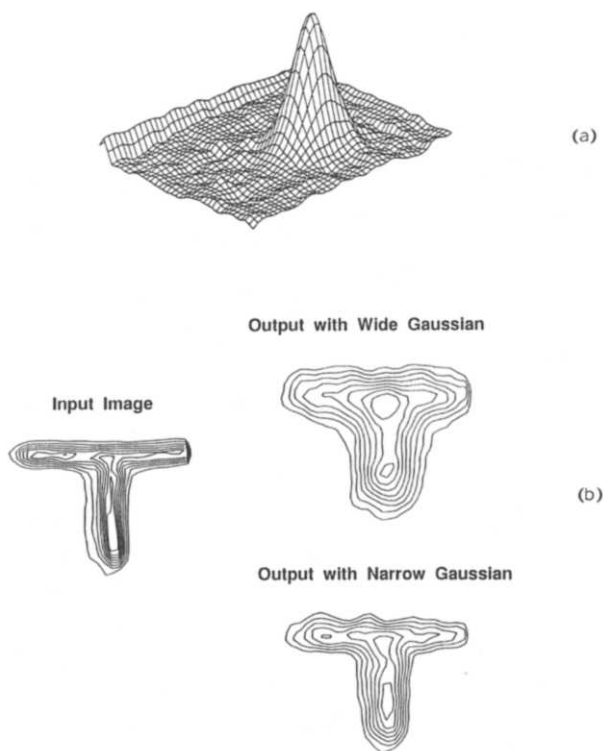


FIGURE 2(a). Measured impulse response; and (b) Smoothed images. Narrow (resp. wide) Gaussian refers to narrow (resp. wide) Gaussian-like kernel for convolution.

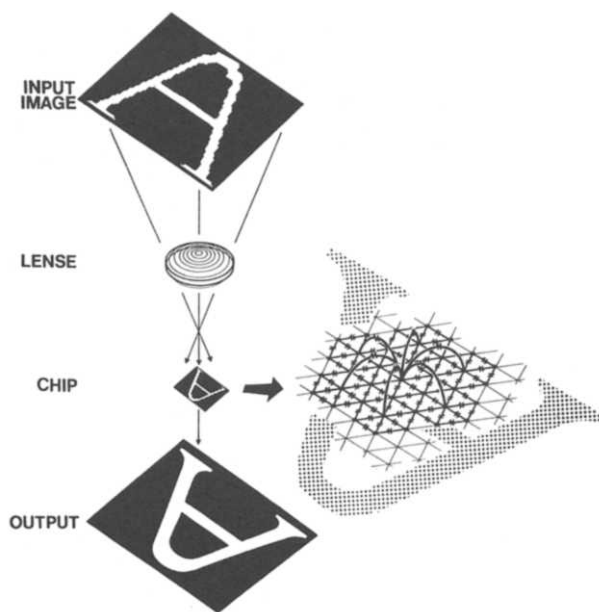


FIGURE 2(c). Schematic diagram.

1. **Stability:** Since $g_2 < 0$ (see Section 2), one has to be very careful about temporal, as well as, spatial stability issues. Although the chip implemented in Kobayashi et al. (1990, 1991) was stable and fully functional, rather elaborate work was necessary to perform a theoretical justification of the spatial, as well as temporal stability (Matsumoto, Kobayashi, & Togawa, 1991, 1992).

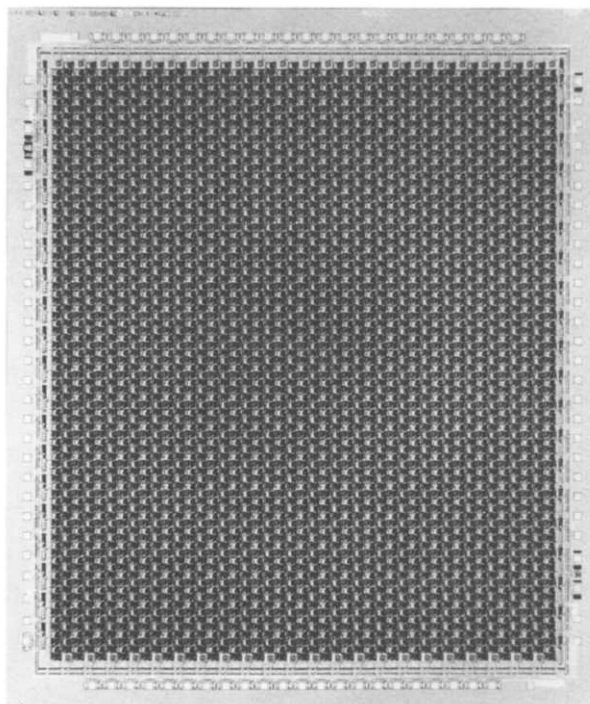


FIGURE 2(d). Chip photograph.

2. **Wiring Complexity:** In Figure 1, only one unit is shown. Since every node has connections with its **second** nearest nodes in addition to the nearest node connections, the actual implementation, excluding the g_0 's is given by Figure 3. This figure naturally explains a high complexity of the wiring. In fact, the wire occupies 47% of the total chip area. Moreover, the architecture of Figure 1 is only a rather crude approximation of the biharmonic operator (see Section 3). A better approximation demands even more wiring. Connections between the third (or farther) nearest nodes are extremely difficult, if not impossible, to implement.

The purpose of this paper is to propose **layered architecture** for regularization problems with higher order smoothness constraints which demands wiring **only** between nearest nodes and requires **no** negative conductance. Section 2 describes the architecture and then shows how the network solves regularization problems. Section 3 explains several aspects associated with two-

dimensional problems. Section 4 shows an application to the *Smoothing-Contrast Enhancement* filter. Section 5 discusses the wiring complexity issue in a quantitative manner. Section 6 explains how the architecture has been inspired by the physiological experiments on lower vertebrate retina performed by one of the authors.

1.2. Related Works

All of the analog early vision chips (Harris, 1988; Harris et al., 1989; Hutchinson et al., 1988; Kobayashi et al., 1990, 1991; Liu & Harris, 1989; Mathur et al., 1990; Mead, 1989; Mead & Mahowald, 1988) have at least one thing in common; massively parallel resistor networks. The networks discussed in this paper are no exception. One of the networks closely related to the networks presented in this paper is the one reported in Kobayashi et al. (1990, 1991) in that it also solves a second order regularization problem, as explained in Section 1.1. There are several important distinctions,

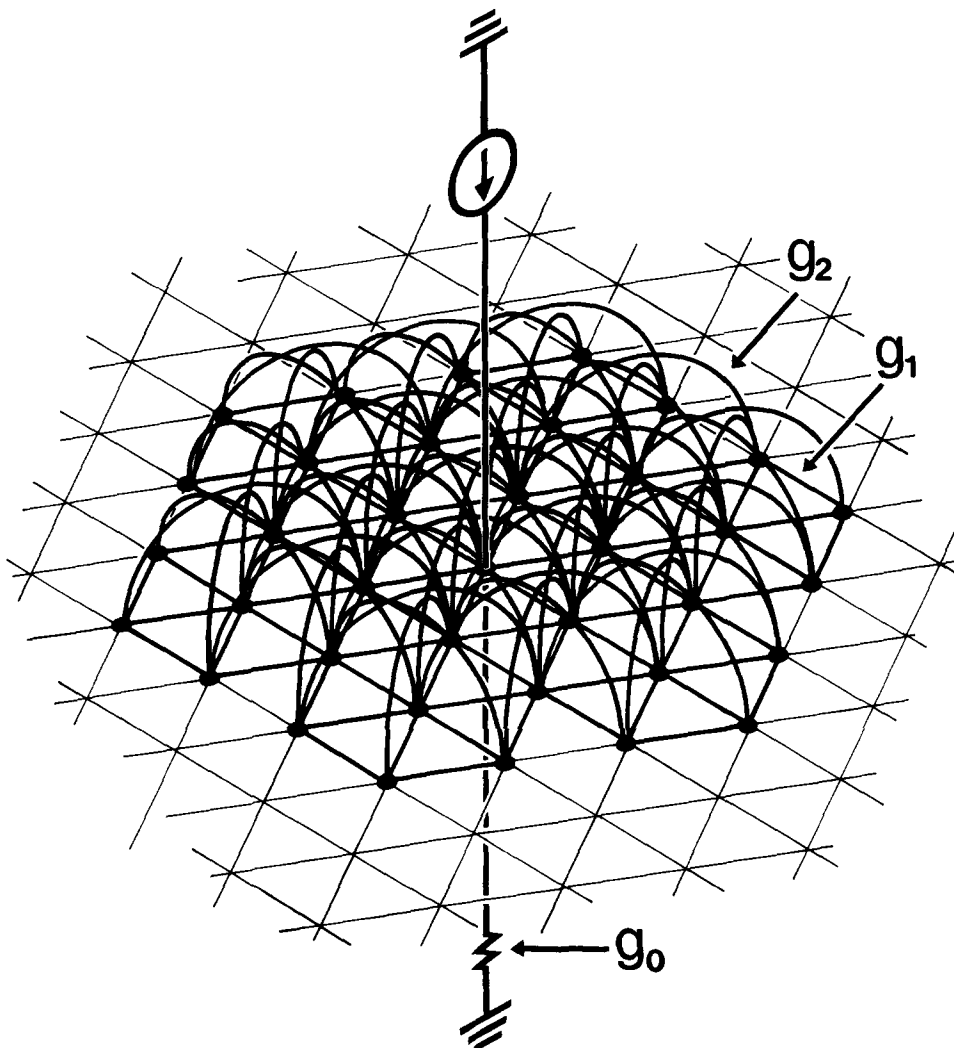


FIGURE 3. Actual implementation demands connections with every second nearest neighbor, in addition to the immediate neighbor connections.

however, which will be explained later. Interesting hierarchical architecture is reported in Harris (1988) and Liu and Harris (1989) for higher order regularization problems. This implementation requires “tri-directional subtract constraint devices.” The architecture given in the next section does not require such devices. It should be noted, however, that the present architecture is not the result of an attempt to improve upon the one in Harris (1988) and Liu and Harris (1989). Rather, it has been inspired by the physiological experiments performed by one of the authors, which will be explained in Section 6. After the completion of this work, the following related works were brought to our attention. K. Uchiyama of NTT VLSI Laboratory pointed out that a layered network with discrete elements, though it is different from ours, is discussed in Yasuda, Yamaguchi, Fukushima, and Nagata (1971). More specific comparative remarks will be given in Section 4. J. Harris of MIT AI Laboratory indicated that in their theses, Terzopoulos (1984) and Harris (1986) also suggested layered resistive networks even though detailed analysis was not performed. Harris also indicated that Suter (1991) has architecture similar to Harris’. This paper is a full account of our earlier results reported in Kobayashi, Matsumoto, Yagi, and Shimmi (1991).

2. ARCHITECTURE

When a solution to an operator equation (not necessarily linear),

$$Av = d, \quad v \in X, \quad d \in Y, \quad (1)$$

loses existence or uniqueness or continuity in d , eqn (1) is called ill-posed. Ill-posedness typically arises when “data” d is noisy, while the solution v sought should be reasonably smooth. It can also result from the nature of A . The Tikhonov regularization (1963a, 1963b, 1965) converts eqn (1) into a family of minimization problems:

$$G(v, d, \lambda) = \|Av - d\|^2 + \lambda\Omega(v) \quad (2)$$

where $\|\cdot\|$ denotes a norm (on Y), $\Omega : X \rightarrow \mathcal{R}$ is continuous and strictly convex, $\lambda > 0$. If $Av^* = d^*$, then under reasonable conditions, eqn (2) regularizes eqn (1) in the sense that for any ϵ -neighborhood $N_\epsilon(v^*)$ of v^* (with respect to an appropriate topology), there is a δ -neighborhood $N_\delta(d^*)$ of d^* such that if $d \in N_\delta(d^*)$, and if $\lambda(\delta) > 0$ is appropriate, then there is a unique $v(d, \lambda(\delta)) \in N_\epsilon(v^*)$ which minimizes eqn (2). It should be noted, however, that when d is noisy, choosing the best λ is another interesting, as well as, difficult problem because one needs to take into account the statistics of d (MacKay, 1991; Whaba, 1987), and it is outside of the scope of this paper.

Now, a typical “stabilizer” $\Omega(v)$ in eqn (2) is of the form

$$\Omega(v) = \sum_{r=1}^P \int_D C_r(\xi) \left(\frac{d^r v(\xi)}{d\xi^r} \right)^2 d\xi \quad (3)$$

where $C_r(\xi) \geq 0$ and $D = [a, b]$ is the domain of the problem. If eqn (2) with eqn (3) can be written as

$$G(v, d, \lambda) = \int_D F(v(\xi), v^{(1)}(\xi), \dots, v^{(P)}(\xi), \xi, d(\xi), \lambda) d\xi, \quad v^{(r)} = \frac{d^r v}{d\xi^r} \quad (4)$$

where F is “well-behaved,” then the variational principle gives the Euler equation

$$\sum_{r=0}^P (-1)^r \frac{d^r}{d\xi^r} \frac{\partial}{\partial v^{(r)}} F(v(\xi), v^{(1)}(\xi), \dots, v^{(P)}(\xi), \xi, d(\xi), \lambda) = 0 \quad (5)$$

with natural boundary conditions:

$$\sum_{r=0}^q (-1)^r \frac{d^r}{d\xi^r} \frac{\partial}{\partial v^{(P-q-r)}} F(v(\xi), v^{(1)}(\xi), \dots, v^{(P)}(\xi), \xi, d(\xi), \lambda) = 0, \quad \text{at } \xi = a, b \text{ for } q = 0, 1, \dots, P. \quad (6)$$

It should be observed that because of the particular form of eqn (3), the Euler equation (5) necessarily contains terms of the form

$$\left(\frac{d^{2r} v}{d\xi^{2r}} \right) (\xi), \quad r = 1, \dots, P. \quad (7)$$

Namely, if the stabilizer (3) contains the r -th order derivative, one needs to implement the **2r-th order** derivative operation for solving the regularization problem.

For the sake of simplicity, the independent variable ξ has been one-dimensional. Two-dimensional problems will be discussed in the next section.

In the following, we will formulate the regularization problem as a minimization problem on a finite dimensional space instead of approximating the Euler equation because

1. In a chip implementation, the space variable ξ takes finite discrete values.
2. The formulation naturally leads to our layered architecture (see Remark after the proof of Fact 1).
3. Discrete approximation of the Euler equation (5) together with the natural boundary condition (6) in a consistent manner is not straightforward. Boundary conditions are important since inadequate boundary conditions even lead to instability (Matsumoto et al., 1991, 1992). Our discrete formulation given below naturally incorporates eqns (5) and (6).
4. Most of the vision chips fabricated/proposed so far, including the filter described in Section 4 of this paper, are on a hexagonal grid instead of a square grid (see Section 3 for reasons). A rigorous approx-

imation result on a hexagonal grid will be rather involved.

Thus, let $\mathbf{v} = (v_1, \dots, v_n)^T \in \mathcal{R}^n$. Then the derivatives in eqn (3) should be replaced by the differences, e.g.,

$$\begin{aligned} \left(\frac{dv}{d\xi}\right)(\xi) &\rightarrow v_k - v_{k-1}, \\ \left(\frac{d^2v}{d\xi^2}\right)(\xi) &\rightarrow v_{k-1} + v_{k+1} - 2v_k. \end{aligned} \quad (8)$$

These operations are conveniently expressed by

$$\left(\frac{dv}{d\xi}\right)(\cdot) \rightarrow \mathbf{D}\mathbf{v}, \quad \left(\frac{d^2v}{d\xi^2}\right)(\cdot) \rightarrow \mathbf{L}\mathbf{v} \quad (9)$$

where

$$\mathbf{D} = \begin{bmatrix} 1 & 0 & 0 & \cdot & \cdot & \cdot & 0 \\ -1 & 1 & 0 & \cdot & \cdot & \cdot & 0 \\ 0 & -1 & 1 & \cdot & \cdot & \cdot & 0 \\ \cdot & \cdot & \cdot & \cdot & \cdot & \cdot & \cdot \\ \cdot & \cdot & \cdot & \cdot & \cdot & \cdot & \cdot \\ 0 & 0 & 0 & \cdot & \cdot & 1 & 0 \\ 0 & 0 & 0 & \cdot & \cdot & -1 & 1 \end{bmatrix}, \quad \mathbf{L} = \begin{bmatrix} -2 & 1 & 0 & \cdot & \cdot & \cdot & 0 \\ 1 & -2 & 1 & \cdot & \cdot & \cdot & 0 \\ 0 & 1 & -2 & \cdot & \cdot & \cdot & 0 \\ \cdot & \cdot & \cdot & \cdot & \cdot & \cdot & \cdot \\ \cdot & \cdot & \cdot & \cdot & \cdot & \cdot & \cdot \\ 0 & 0 & 0 & \cdot & \cdot & -2 & 1 \\ 0 & 0 & 0 & \cdot & \cdot & 1 & -2 \end{bmatrix} \quad (10)$$

Note that although \mathbf{D} is not symmetric, $\mathbf{D}^T\mathbf{D}$ is symmetric and

$$\mathbf{D}^T\mathbf{D} = -\mathbf{L} \quad (11)$$

where T denotes transpose of matrix. Therefore, the regularization problem for finite dimensional space case calls for minimizing

$$\begin{aligned} G(\mathbf{v}, \mathbf{d}, \lambda) &= \|\mathbf{A}\mathbf{v} - \mathbf{d}\|^2 \\ &+ \lambda \sum_{r=1}^P \begin{cases} \sum_k C_r(k)(\mathbf{L}^{r/2}\mathbf{v})_k^2 & r: \text{even} \\ \sum_k C_r(k)(\mathbf{D}\mathbf{L}^{r-1/2}\mathbf{v})_k^2 & r: \text{odd} \end{cases} \end{aligned} \quad (12)$$

where $\mathbf{d} = (d_1, \dots, d_n)^T \in \mathcal{R}^n$, $C_r(k) \geq 0$ and $(\mathbf{L}^{r/2}\mathbf{v})_k$ (respectively $(\mathbf{D}\mathbf{L}^{r-1/2}\mathbf{v})_k$) is the k -th component of $\mathbf{L}^{r/2}\mathbf{v}$ (respectively $\mathbf{D}\mathbf{L}^{r-1/2}\mathbf{v}$).

This discrete formulation:

1. automatically takes care of the natural boundary conditions because the summation over k in (12) at the boundary reflects the boundary conditions (a similar argument is used in Terzopoulos (1984) and Grimson (1981)), and
2. explains our layered architecture in a transparent manner (see Remark after Fact 1).

In this paper, we have no intention of solving all the regularization problems. Rather, we will restrict ourselves to the class of regularization problems where (a) $\mathbf{A} = \mathbf{1}$, identity matrix; and (b) $C_r(k)$ is independent

of the space variable k . Various generalizations are possible. Sparse data problem, for instance, gives rise to an \mathbf{A} which is a projection operator of \mathcal{R}^n onto its proper subspace and it leads to a rather interesting architecture. This will be reported elsewhere. Note that (b) is very mild.

Minimization of eqn (12) will be called the **P-th order regularization problem**. Since \mathbf{L} is negative definite, (hence $-\mathbf{L}$ is positive definite), the minimization problem has a unique solution given by

$$\frac{\partial G}{\partial \mathbf{v}} = \mathbf{v} - \mathbf{d} + \sum_{r=1}^P (-1)^r \lambda_r \mathbf{L}^r \mathbf{v} = \mathbf{0}, \quad \lambda_r := \lambda C_r \quad (13)$$

where eqn (11) was used (compare with eqn (5)).

Note that if $\lambda_r \neq 0$, then the solution (13) necessarily contains the $\mathbf{L}^r \mathbf{v}$ term. This corresponds to the presence of the $(d^{2r}v/d\xi^{2r})(\xi)$ term in the infinite dimensional case. Most of the neuro chips fabricated so far are for $P = 1$ with one of the very few exceptions, to the best of our knowledge, being the Gaussian-like convolver chip (Kobayashi et al., 1990, 1991) where $P = 2$, $\lambda_2 \neq 0$, $\lambda_1 = 0$. Another exception is reported in Harris (1988). It has been known that regularizations with $P = 2$ often perform better than those with $P = 1$. In order to see the differences between $P = 1$ and $P > 1$, first note that eqn (13) with $P = 1$ reads

$$\mathbf{v} - \mathbf{d} - \lambda_1 \mathbf{L}\mathbf{v} = \mathbf{0}. \quad (14)$$

It is well known that this can be implemented by a parallel network where each node is connected with only its nearest neighbors via passive conductance. Next, consider $P = 2$, $\lambda_2 \neq 0$, $\lambda_1 = 0$, which amounts to

$$\mathbf{v} - \mathbf{d} + \lambda_2 \mathbf{L}^2 \mathbf{v} = \mathbf{0}. \quad (15)$$

Note that

$$\begin{aligned} \mathbf{L}^2 &= \begin{bmatrix} -2 & 1 & 0 & 0 & \cdot & \cdot & \cdot & 0 \\ 1 & -2 & 1 & 0 & \cdot & \cdot & \cdot & 0 \\ 0 & 1 & -2 & 1 & \cdot & \cdot & \cdot & 0 \\ \cdot & \cdot \\ \cdot & \cdot \\ 0 & 0 & 0 & \cdot & \cdot & 1 & -2 & 1 \\ 0 & 0 & 0 & \cdot & \cdot & 0 & 1 & -2 \end{bmatrix} \\ &\times \begin{bmatrix} -2 & 1 & 0 & 0 & \cdot & \cdot & \cdot & 0 \\ 1 & -2 & 1 & 0 & \cdot & \cdot & \cdot & 0 \\ 0 & 1 & -2 & 1 & \cdot & \cdot & \cdot & 0 \\ \cdot & \cdot \\ \cdot & \cdot \\ 0 & 0 & 0 & \cdot & \cdot & 1 & -2 & 1 \\ 0 & 0 & 0 & \cdot & \cdot & 0 & 1 & -2 \end{bmatrix} \\ &= \begin{bmatrix} * & -4 & 1 & 0 & \cdot & \cdot & \cdot & 0 \\ -4 & 6 & -4 & 1 & \cdot & \cdot & \cdot & 0 \\ 1 & -4 & 6 & -4 & \cdot & \cdot & \cdot & 0 \\ \cdot & \cdot \\ \cdot & \cdot \\ 0 & 0 & 0 & \cdot & \cdot & -4 & 6 & -4 \\ 0 & 0 & 0 & \cdot & \cdot & 1 & -4 & * \end{bmatrix} \end{aligned} \quad (16)$$

where $\ast = 5$ due to the ‘‘boundary effect.’’ One sees that the k -th component of eqn (15) in the ‘‘interior’’ reads

$$v_k - d_k + \lambda_2[6v_k - 4(v_{k-1} + v_{k+1}) + v_{k-2} + v_{k+2}] = 0. \quad (17)$$

A direct implementation of eqn (17) is given by Figure 4 (Figure 1 is a two-dimensional version) where

$$g_0, g_1 > 0, \quad g_2 < 0, \quad g_1 = 4|g_2| \quad (18)$$

because the Kirchoff Current Law (KCL) gives

$$-(g_0 + 2g_1 + 2g_2)v_k + g_1(v_{k-1} + v_{k+1}) + g_2(v_{k-2} + v_{k+2}) + u_k = 0. \quad (19)$$

Therefore, $\lambda_2 = g_0/|g_2|$, $d_k = \lambda_2 u_k$. This is what has been done in Kobayashi et al. (1990, 1991) and in Harris (1988). For a general r , the matrix L^r is of the form

$$L^r = \begin{bmatrix} a_0 & a_1 & a_2 & \cdot & a_r & 0 & 0 & \cdot & \cdot & 0 \\ a_1 & a_0 & a_1 & a_2 & \cdot & a_r & 0 & \cdot & \cdot & 0 \\ a_2 & a_1 & a_0 & a_1 & \cdot & \cdot & \cdot & \cdot & \cdot & 0 \\ \cdot & a_2 & a_1 & a_0 & \cdot & \cdot & \cdot & \cdot & \cdot & 0 \\ a_r & \cdot & a_r & 0 \\ 0 & a_r & \cdot & a_r \\ 0 & 0 & \cdot & \cdot & \cdot & \cdot & a_0 & a_1 & a_2 & \cdot \\ \cdot & \cdot & \cdot & \cdot & \cdot & \cdot & a_1 & a_0 & a_1 & a_2 \\ 0 & \cdot & \cdot & 0 & a_r & \cdot & a_2 & a_1 & a_0 & a_1 \\ 0 & \cdot & \cdot & 0 & 0 & a_r & \cdot & a_2 & a_1 & a_0 \end{bmatrix} \quad (20)$$

where the boundary effects are not explicitly shown in order to save the space. Equation (20) shows that direct implementation requires connections between every pair of the k -th nearest nodes for all $k \leq r$ with possibly negative conductance. As was remarked, $r = 2$ is already very difficult. The architecture given below solves the P -th order regularization problem with only wiring between nearest nodes and without negative conductance. The following fact shows that the network given by Figure 5 (in one-dimension) solves the P -th order regu-

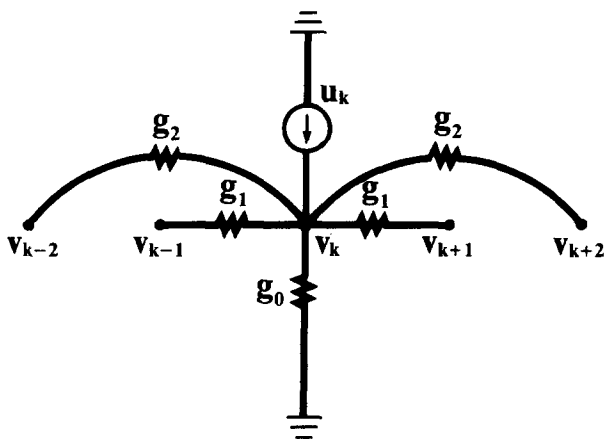


FIGURE 4. Implementation of the 4th order derivative.

larization problem for all P , $1 \leq P \leq N$, simultaneously. Two-dimensional problems will be discussed in Section 3.

Fact 1. Consider the network given by Figure 5(a) (in one-dimension) where the symbol given in Figure 5(b) stands for a voltage controlled current source, and $g_{m_i}, g_{s_i} > 0, i = 1, \dots, N$.

1. The network is temporally stable in the sense that for any symmetric positive definite (not necessarily diagonal) parasitic capacitance matrix, the temporal dynamics converges to a unique stable equilibrium for any DC input.
2. At an equilibrium, the voltage distribution of the P -th layer, $1 \leq P \leq N$, simultaneously solves the P -th order regularization with

$$\lambda_P = \frac{g_{s_1} \cdots g_{s_P}}{g_{m_1} \cdots g_{m_P}} \quad (21)$$

$$\lambda_{P-1} = \frac{g_{s_1} \cdots g_{s_{P-1}} g_{m_P} + g_{s_1} \cdots g_{s_{P-2}} g_{m_{P-1}} g_{s_P} + \cdots + g_{m_1} g_{s_2} \cdots g_{s_P}}{g_{m_1} \cdots g_{m_P}} \quad (22)$$

$$\lambda_{P-2} = \frac{g_{s_1} \cdots g_{s_{P-2}} g_{m_{P-1}} g_{m_P} + g_{s_1} \cdots g_{s_P} g_{m_{P-2}} g_{m_{P-1}} g_{s_P} + \cdots + g_{m_1} g_{m_2} g_{s_3} \cdots g_{s_P}}{g_{m_1} \cdots g_{m_P}} \quad (23)$$

$$\lambda_1 = \frac{g_{m_1} \cdots g_{m_{P-1}} g_{s_P} + g_{m_1} \cdots g_{m_{P-2}} g_{s_{P-1}} g_{m_P} + \cdots + g_{s_1} g_{m_2} \cdots g_{m_P}}{g_{m_1} \cdots g_{m_P}} \quad (24)$$

$$d_k = \frac{T_1 \cdots T_{P-1}}{g_{m_1} \cdots g_{m_P}} u_k. \quad (25)$$

3. The voltage distributions of all the layers are spatially stable in the sense of Matsumoto et al. (1991, 1992).

Proof. (a) In order to prove the temporal stability, consider the temporal dynamics of the voltage distribution $v^1(t) \in \mathcal{R}^n$ of the first layer:

$$C^1 \frac{dv^1(t)}{dt} = (g_{s_1} L - g_{m_1} \mathbf{1}) v^1(t) + u(t) \quad (26)$$

where L is defined by eqn (10) and C^1 is the parasitic capacitance matrix (not necessarily diagonal). Similarly, the i -th layer ($2 \leq i \leq N$) temporal dynamics is described by

$$C^i \frac{dv^i(t)}{dt} = (g_{s_i} L - g_{m_i} \mathbf{1}) v^i(t) + T_{i-1} v^{i-1}(t). \quad (27)$$

Note that the first layer is ‘‘decoupled’’ from the rest of the network because the voltage controlled current source $T_1 v^1(t)$ is a unilateral element, i.e., there is no feedback from the second or other layers to the first layer. Since $g_{s_1} > 0$, it is easy to show that $(g_{s_1} L - g_{m_1} \mathbf{1})$ is negative definite because $g_{m_1} > 0$. Therefore,

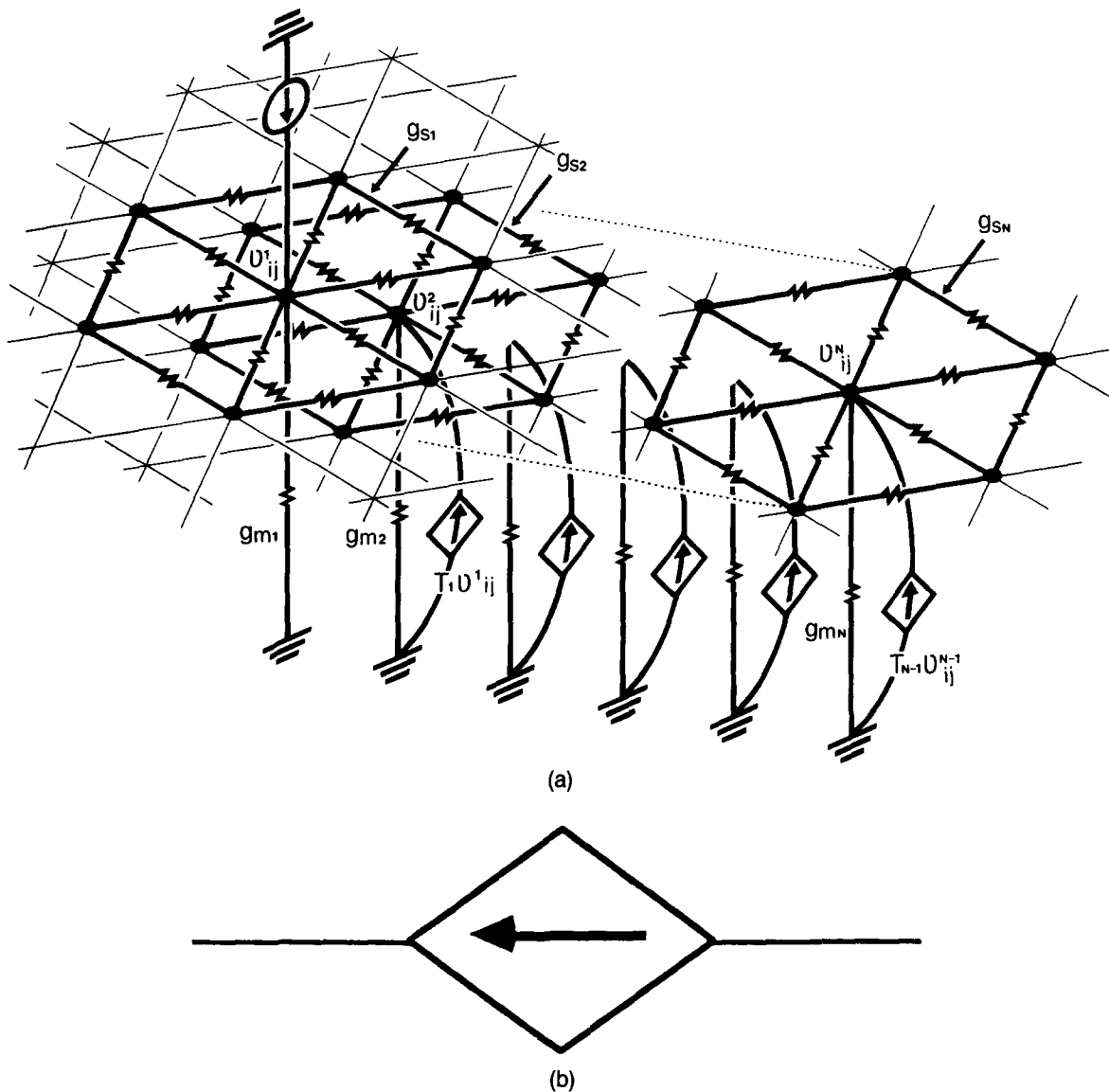


FIGURE 5(a). The layered architecture; and (b) Voltage controlled current source.

$\mathbf{v}^1(t)$ converges to a stable equilibrium exponentially. Since the second layer has exactly the same structure as the first layer, except for the fact that $\mathbf{u}(t)$ is replaced with $T_1 \mathbf{v}^1(t)$, and since $\mathbf{v}^1(t)$ is exponentially convergent, $\mathbf{v}^2(t)$ also converges exponentially. Therefore, at these stable equilibria, the network satisfies

$$(g_{m_1} \mathbf{1} - g_{s_1} \mathbf{L}) \mathbf{v}^1 - \mathbf{u} = \mathbf{0} \quad (28)$$

$$(g_{m_i} \mathbf{1} - g_{s_i} \mathbf{L}) \mathbf{v}^i - T_{i-1} \mathbf{v}^{i-1} = \mathbf{0}, \quad 2 \leq i \leq N. \quad (29)$$

Recall eqn (13), which is the solution for the regularization problem. For $P = 1$, it is clear that eqn (28) solves the first order regularization with $\lambda_1 = g_{s_1}/g_{m_1}$ and $\mathbf{d} = (1/g_{m_1})\mathbf{u}$. Let $2 \leq P \leq N$. Then a successive substitution of eqn (29) into eqn (28) gives

$$(g_{m_1} \mathbf{1} - g_{s_1} \mathbf{L})(g_{m_2} \mathbf{1} - g_{s_2} \mathbf{L}) \dots (g_{m_P} \mathbf{1} - g_{s_P} \mathbf{L}) \mathbf{v}^P - T_1 \dots T_{P-1} \mathbf{u} = \mathbf{0} \quad (30)$$

which amounts to

$$\begin{aligned} & (-1)^P g_{s_1} \dots g_{s_P} \mathbf{L}^P \mathbf{v}^P + (-1)^{P-1} (g_{s_1} \dots g_{s_{P-1}} g_{m_P} \\ & + g_{s_1} \dots g_{s_{P-2}} g_{s_P} g_{m_{P-1}} + \dots) \mathbf{L}^{P-1} \mathbf{v}^P + \dots \\ & - (g_{m_1} \dots g_{m_{P-1}} g_{s_P} + g_{m_1} \dots g_{m_{P-2}} g_{m_P} g_{s_{P-1}} + \dots) \mathbf{L} \mathbf{v}^P \\ & + g_{m_1} \dots g_{m_P} \mathbf{1} \mathbf{v}^P - T_1 \dots T_{P-1} \mathbf{u} = \mathbf{0}. \quad (31) \end{aligned}$$

Comparing this equation with eqn (13), one has eqns (21)–(25).

(b) One can easily show that all the layers satisfy the spatial stability condition given in Matsumoto et al. (1991, 1992). ■

REMARKS. (a) The idea behind our architecture is extremely simple. The concatenation structure $\mathbf{L}' = \mathbf{L} \mathbf{L} \dots \mathbf{L}$ naturally maps into the layered network of Figure 5(a). Consider the network given by Figure 6 where KCL gives

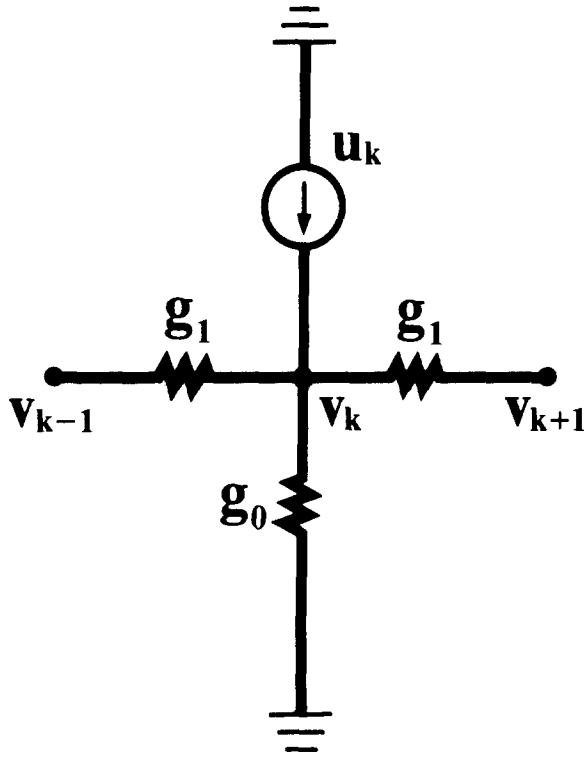


FIGURE 6. The 2nd order derivative.

$$-2v_k + v_{k-1} + v_{k+1} - \frac{g_m}{g_s} v_k = \frac{1}{g_s} d_k. \quad (32)$$

If g_m/g_s is small, then eqn (32) roughly amounts to

$$\mathbf{L}v^1 \approx \mathbf{u} \quad (33)$$

The second layer receives $T_1 v^1$ as input, and solves

$$\mathbf{L}v^2 \approx T_1 v^1 \quad (34)$$

and similarly

$$\mathbf{L}v^i \approx T_{i-1} v^{i-1} \quad (35)$$

which gives

$$\mathbf{L}^i v^i \approx T_1 \dots T_{i-1} \mathbf{u}. \quad (36)$$

(b) Observe that the weights $\lambda_P, \dots, \lambda_1$ are explicitly given as functions of the conductance values. (c) In our discrete formulation (12), conditions corresponding to the natural boundary conditions for the Euler equation are reflected in the boundary elements of the matrices \mathbf{D} and \mathbf{L} .

Is the multilayered network completely equivalent to a single-layer network with negative conductance?

The answer is no. In order to see this, recall Fact 1 and let

$$\psi : (g_{m_1}, \dots, g_{m_P}, g_{s_1}, \dots, g_{s_P}) \rightarrow (\lambda_1, \dots, \lambda_P) \quad (37)$$

be the map: $\mathcal{R}^{2P} \rightarrow \mathcal{R}^P$ defined by eqns (21)–(25). If ψ is a surjection, then the multilayered network can solve every problem solved by a single-layer network with negative conductances, $\mathbf{A} = \mathbf{I}$. Even though there are twice as many parameters ($g_{m_1}, \dots, g_{m_P}, g_{s_1}, \dots, g_{s_P}$) in the layered network as in a single-layer network, ψ is not surjective. It is easy to show that the layered network cannot solve the pure P -th order regularization problem, i.e., $\lambda_P \neq 0$, and $\lambda_r = 0$ for all other $r \neq P$. Whether this is harmful for the layered network is another issue, however. Let us look at the $P = 2$ problem. Figure 7(a) shows the impulse response of the single layer network of Figure 4 where $1/g_0 = 200 \text{ k}\Omega$, $1/g_1 = 5 \text{ k}\Omega$, $1/g_2 = -20 \text{ k}\Omega$ so that $g_1 : g_2 = 4 : -1$ and hence, $\lambda_1 = 0$. Figure 7(b) shows the impulse response of the layered network with $P = 2$, and $1/g_{m_1} = 800 \text{ k}\Omega$, $1/g_{m_2} = 500 \text{ k}\Omega$, $1/g_{s_1} = 80 \text{ k}\Omega$, $1/g_{s_2} = 450 \text{ k}\Omega$, $T_1 = 2 \mu\text{Siemens}$. Since $\lambda_1 = g_{s_1}/g_{m_1} + g_{s_2}/g_{m_2}$ (see eqn (24)), it cannot be zero. The problem with $\lambda_1 = 0$ is called the *thin plate* while the problem with $\lambda_1 \neq 0$ is called the *thin plate under tension* (Terzopoulos, 1984). Observe the slight negative response in Figure 7(a) while there is no negative response in Figure 7(b). The latter is a consequence of the fact that no negative conductances are involved. Because of the negative response, the thin plate does not really correspond to Gaussian convolution although they are close. There is an interesting distinction between the $\lambda_1 = 0$ case and the $\lambda_1 \neq 0$ case when data is sparse. This will be reported elsewhere.

Let us characterize the responses of Figure 7(a) and Figure 7(b) analytically. Observe that one can recast eqn (19) as

$$\mathbf{x}_{k+1} = \mathbf{F}\mathbf{x}_k + \mathbf{y}_k \quad (38)$$

where

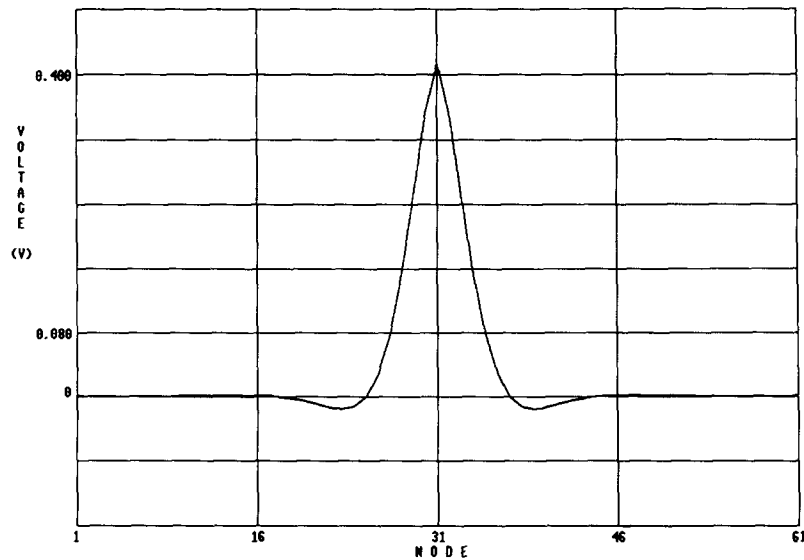
$$\mathbf{F} = \begin{bmatrix} 0 & 1 & 0 & 0 \\ 0 & 0 & 1 & 0 \\ 0 & 0 & 0 & 1 \\ -1 & -g_1/g_2 & (g_0 + 2g_1 + 2g_2)/g_2 & -g_1/g_2 \end{bmatrix} \quad (39)$$

$$\mathbf{x}_k = (v_{k-2}, v_{k-1}, v_k, v_{k+1})^T \quad (40)$$

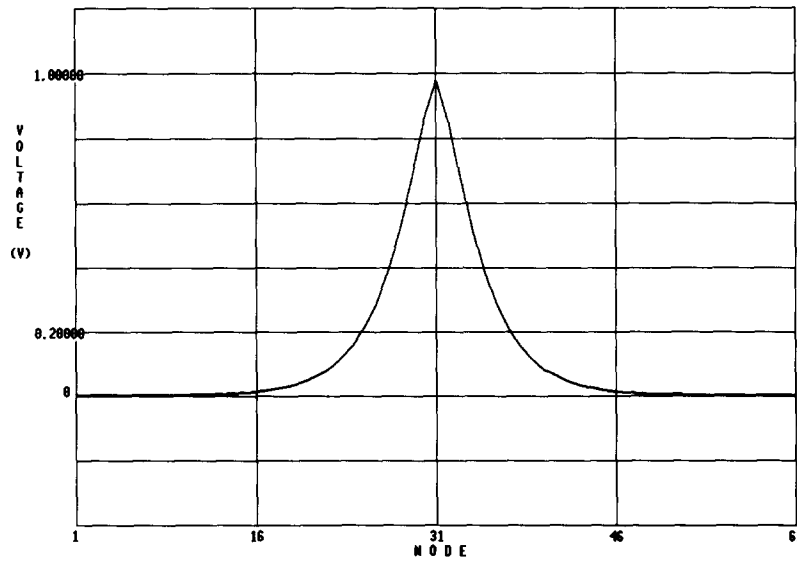
$$\mathbf{y}_k = (0, 0, 0, -u_k/g_2)^T. \quad (41)$$

On the other hand, for the layered network, one can show that the second layer voltage distribution is described by eqn (38) where \mathbf{F} is now replaced by

$$\mathbf{F} = \begin{bmatrix} 0 & 1 & 0 & 0 \\ 0 & 0 & 1 & 0 \\ 0 & 0 & 0 & 1 \\ -1 & 4 + g_{m_1}/g_{s_1} + g_{m_2}/g_{s_2} & -6 - 2g_{m_1}/g_{s_1} - 2g_{m_2}/g_{s_2} & 4 + g_{m_1}/g_{s_1} + g_{m_2}/g_{s_2} \end{bmatrix}. \quad (42)$$



(a)



(b)

FIGURE 7. Impulse response (a) eqn 39; and (b) eqn 42.

Equation (38) with eqn (39) is the “spatial” dynamics of the network of Figure 4 representing how the node voltage v_k is distributed in response to u_k . Similarly, eqn (38) with eqn (42) is the spatial dynamics of v_k^2 of the layered network. Since eqn (38) is a discrete linear dynamical system, its behavior is completely characterized by the eigenvalues of F .

Fact 2. (a) The eigenvalues of F defined by eqn (39) are two sets of *complex-conjugate* pairs off the unit circle in the complex plane such that $r e^{\pm j\theta}$, $r^{-1} e^{\pm j\theta}$, $r > 0$, $\theta \neq 0, \pi$ (Figure 8(a)). (b) The eigenvalues of F defined by eqn (42) are *four reals* off the unit circle in the complex plane such that $r_1, r_2, r_1^{-1}, r_2^{-1}$, $r_1, r_2 \neq 0, r_1 \neq r_2$ (Figure 8(b)).

Proof. The proof utilizes our general result on matrices of the form

$$F = \begin{bmatrix} 0 & 1 & 0 & 0 & \cdot & \cdot & 0 \\ 0 & 0 & 1 & 0 & \cdot & \cdot & 0 \\ 0 & 0 & 0 & 1 & \cdot & \cdot & 0 \\ \cdot & \cdot & \cdot & \cdot & \cdot & \cdot & \cdot \\ \cdot & \cdot & \cdot & \cdot & \cdot & \cdot & \cdot \\ 0 & 0 & 0 & \cdot & \cdot & 0 & 1 \\ -1 & -a_{P-1} & -a_{P-2} & \cdot & -a_0 & \cdot & -a_{P-1} \end{bmatrix} \quad (43)$$

which describes the behavior of a general class of networks including P -th order regularization network (Matsumoto et al., 1991).

For $P = 2$, matrix F is 4×4 and the four eigenvalues are given by

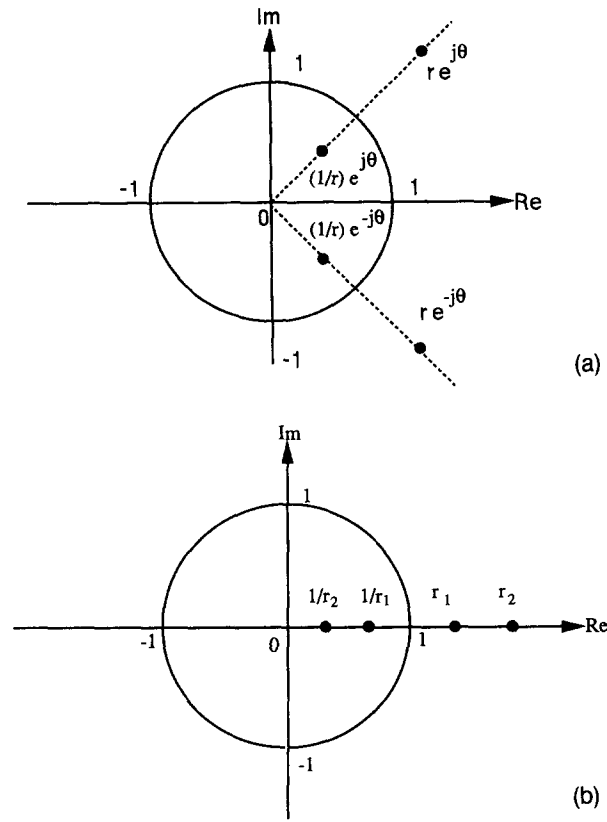


FIGURE 8. Eigenvalue configuration of F . (a) eqn 39; and (b) eqn 42.

$$\frac{1}{2}(\omega_1 \pm \sqrt{\omega_1^2 - 4}), \frac{1}{2}(\omega_2 \pm \sqrt{\omega_2^2 - 4}) \quad (44)$$

where ω_1 and ω_2 are the zeros of

$$Q(\omega) := \omega^2 + a_1\omega + a_0 - 2. \quad (45)$$

One can easily show that if

$$a_0 > 2 + \frac{1}{4}a_1^2 \quad (46)$$

then statement (a) of Fact 2 holds. On the other hand, if

$$-\frac{1}{2}a_0 - 1 < a_1 < -4 \quad \text{and} \quad a_0 < 2 + \frac{1}{2}a_1^2 \quad (47)$$

then statement (b) of Fact 2 is valid. For the F -matrix of eqn (39) (recall eqn (18))

$$a_1 = -4, \quad a_0 = 6 + \frac{g_0}{|g_2|} \quad (48)$$

so that

$$6 + \frac{g_0}{|g_2|} > 2 + \frac{1}{4}(4)^2 \quad (49)$$

and hence, eqn (46) holds. For the F -matrix defined by eqn (42),

$$a_1 = -\left(4 + \frac{g_{m_1}}{g_{s_1}} + \frac{g_{m_2}}{g_{s_2}}\right), \quad a_0 = 6 + 2\frac{g_{m_1}}{g_{s_1}} + 2\frac{g_{m_2}}{g_{s_2}}. \quad (50)$$

One can easily show that eqn (47) is satisfied. ■

3. TWO-DIMENSIONAL PROBLEMS

Although the basic idea of our layered architecture derived in the previous section is naturally carried over to two-dimensional problems, there are three issues which call for explanations. First, when there are two independent space variables, say ξ and η , there is more than one choice of the stabilizer (3). With $P = 2$, for instance, the stabilizer can be

$$\lambda \iint (v_{\xi\xi} + v_{\eta\eta})^2 d\xi\eta \quad (51)$$

or

$$\lambda \iint (v_{\xi\xi}^2 + 2v_{\xi\eta}^2 + v_{\eta\eta}^2) d\xi\eta \quad (52)$$

or other forms, where

$$v_{\xi\xi} = \frac{\partial^2 v}{\partial \xi^2}, \quad v_{\xi\eta} = \frac{\partial^2 v}{\partial \xi \partial \eta}, \quad v_{\eta\eta} = \frac{\partial^2 v}{\partial \eta^2}. \quad (53)$$

Second, natural boundary conditions get more involved. For instance, if $P = 2$ and $\lambda_1 = 0$, then the first variation of

$$G(v, d, \lambda) = \iint_D F(v(\xi, \eta), v_{\xi\xi}, v_{\xi\eta}, v_{\eta\eta}, \xi, \eta, d(\xi, \eta), \lambda) d\xi d\eta \quad (54)$$

on the boundary ∂D gives rise to

$$\int_{\partial D} \left[\psi_\xi \left(\frac{\partial F}{\partial v_{\xi\xi}} - \frac{1}{2} \frac{\partial F}{\partial v_{\xi\eta}} \right) - \psi \frac{\partial}{\partial \xi} \left(\frac{\partial F}{\partial v_{\xi\xi}} - \frac{1}{2} \frac{\partial F}{\partial v_{\xi\eta}} \right) \right] d\eta - \int_{\partial D} \left[\psi_\eta \left(\frac{\partial F}{\partial v_{\eta\eta}} - \frac{1}{2} \frac{\partial F}{\partial v_{\xi\eta}} \right) - \psi \frac{\partial}{\partial \eta} \left(\frac{\partial F}{\partial v_{\eta\eta}} - \frac{1}{2} \frac{\partial F}{\partial v_{\xi\eta}} \right) \right] d\xi \quad (55)$$

where $v(\xi, \eta)$ is perturbed to $v(\xi, \eta) + \psi(\xi, \eta)$. When one performs integration by parts on ∂D , one obtains, for instance, for eqn (52)

$$-(v_{\eta\eta} + v_{\xi\xi}) + (v_{\xi\xi}\xi_\tau^2 + 2v_{\xi\eta}\xi_\tau\eta_\tau + v_{\eta\eta}\eta_\tau^2) = 0 \quad (56)$$

$$\frac{\partial}{\partial n} (v_{\eta\eta} + v_{\xi\xi}) + \frac{\partial}{\partial \tau} (v_{\xi\xi}\xi_n\xi_\tau + v_{\xi\eta}(\xi_n\eta_\tau + \xi_\tau\eta_n) + v_{\eta\eta}\eta_n\eta_\tau) = 0 \quad (57)$$

on ∂D where ξ_n, η_n and ξ_τ, η_τ are the direction cosines of the outward normal and the tangent vectors, respectively. Approximation consistent with eqns (56) and (57) together with Euler equation

$$\frac{\partial F}{\partial v} + \frac{\partial^2}{\partial \xi^2} \frac{\partial F}{\partial v_{\xi\xi}} + \frac{\partial^2}{\partial \xi \partial \eta} \frac{\partial F}{\partial v_{\xi\eta}} + \frac{\partial^2}{\partial \eta^2} \frac{\partial F}{\partial v_{\eta\eta}} = 0 \quad (58)$$

will not be easy to justify rigorously.

Third, many of the vision chips implemented or proposed so far including the one described in Section 4 of this paper are on a hexagonal grid because

1. A network on a hexagonal grid has much better circular symmetry than on a square grid (Kobayashi et al., 1991; Mead, 1989).

2. A hexagonal grid affords the greatest spatial sampling efficiency in the sense that the least number of nodes will attain a desired coverage of the image (Dudgeon & Mersereau, 1984).

We will handle the problem as a minimization problem on a finite dimensional space as was in eqn (12). It should be noted that in our arguments below, everything is rigorous in so far as the minimization is concerned.

On a hexagonal grid there are two labeling conventions; standard grid (Figure 9(a)) and alternate grid (9(b)). We will use the standard grid. Let

$$\mathbf{v} := (v_{11}, v_{12}, \dots, v_{1n}, v_{21}, v_{22}, \dots, v_{2n}, \dots, v_{n1}, v_{n2}, \dots, v_{nn}) \in \mathcal{R}^{n \times n} \quad (59)$$

and let \mathbf{d} be similarly defined.

1. $P = 1$. The most reasonable function to minimize is

$$G(\mathbf{v}, \mathbf{d}, \lambda_1) = \|\mathbf{v} - \mathbf{d}\|^2 + \lambda_1 (\|\mathbf{D}_1 \mathbf{v}\|^2 + \|\mathbf{D}_2 \mathbf{v}\|^2 + \|\mathbf{D}_3 \mathbf{v}\|^2) \quad (60)$$

where the (i, j) -th component of $\mathbf{D}_1 \mathbf{v}$, $\mathbf{D}_2 \mathbf{v}$ and $\mathbf{D}_3 \mathbf{v}$ are, respectively, given by

$$(\mathbf{D}_1 \mathbf{v})_{ij} = v_{ij} - v_{i-1,j} \quad (61)$$

$$(\mathbf{D}_2 \mathbf{v})_{ij} = v_{ij} - v_{i,j-1} \quad (62)$$

$$(\mathbf{D}_3 \mathbf{v})_{ij} = v_{ij} - v_{i-1,j+1}. \quad (63)$$

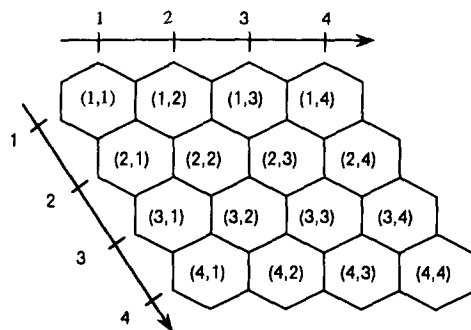
Appropriate modifications must be made on the boundary. Differentiation of eqn (60) with respect to \mathbf{v} gives

$$\mathbf{v} - \mathbf{d} - \lambda_1 \mathbf{L} \mathbf{v} = \mathbf{0} \quad (64)$$

where

$$\mathbf{L} := -(\mathbf{D}_1^T \mathbf{D}_1 + \mathbf{D}_2^T \mathbf{D}_2 + \mathbf{D}_3^T \mathbf{D}_3). \quad (65)$$

Equation (64) is of exactly the same form as in eqn (14), where L is now replaced by eqn (65). The (i, j) -th component of $\mathbf{L} \mathbf{v}$ in the interior reads



(a)

$$v_{i-1,j} + v_{i+1,j} + v_{i,j-1} + v_{i,j+1} + v_{i-1,j+1} + v_{i+1,j-1} - 6v_{i,j}, \quad (66)$$

which is a reasonable approximation of the Laplacian on a hexagonal grid. One can easily show that eqn (64) corresponds to the KCL of the network shown in Figure 5 with $P = 1$.

2. $P = 2$. As was remarked earlier, there are more than one reasonable choices of G .

2(a).

$$G(\mathbf{v}, \mathbf{d}, \lambda_1, \lambda_2) = \|\mathbf{v} - \mathbf{d}\|^2 + \lambda_1 (\|\mathbf{D}_1 \mathbf{v}\|^2 + \|\mathbf{D}_2 \mathbf{v}\|^2 + \|\mathbf{D}_3 \mathbf{v}\|^2) + \lambda_2 \|\mathbf{L} \mathbf{v}\|^2 \quad (67)$$

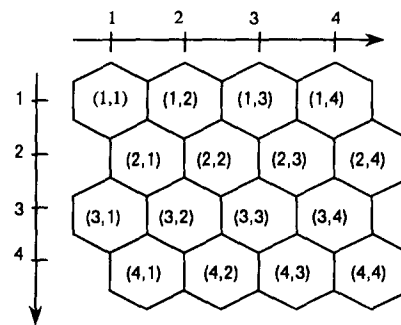
where \mathbf{L} is defined by eqn (65). The solution to this problem is given by

$$\mathbf{v} - \mathbf{d} - \lambda_1 \mathbf{L} \mathbf{v} + \lambda_2 \mathbf{L}^2 \mathbf{v} = \mathbf{0} \quad (68)$$

which, again, is of the form (12). The (i, j) -th component of $\mathbf{L}^2 \mathbf{v}$ in the interior reads

$$v_{i-2,j} + v_{i+2,j} + v_{i,j-2} + v_{i,j+2} + v_{i-2,j+2} + v_{i+2,j-2} + 2(v_{i-1,j-1} + v_{i+1,j+1} + v_{i-1,j+2} + v_{i+1,j-2} + v_{i-2,j+1} + v_{i+2,j-1}) - 10(v_{i-1,j} + v_{i+1,j} + v_{i,j-1} + v_{i,j+1} + v_{i-1,j+1} + v_{i+1,j-1}) + 42v_{i,j}, \quad (69)$$

which is a reasonable approximation of the biharmonic operator on a hexagonal grid. Note that the third term $\lambda_2 \|\mathbf{L} \mathbf{v}\|^2$ in eqn (68) corresponds to a solution with eqn (51) which is called the square Laplacian (Grimson, 1981). The question as to what would be a good approximation of the quadratic variation (52) (Grimson, 1981) on a hexagonal grid may not be easy to answer. We will not pursue this subject since it is not our purpose in this paper. Grimson (1981) observed a difference between solutions to a particular visual reconstruction problem (not regularization problem) with constraints (51) and (52). We have, so far, observed no strange behavior to the solution to eqn (67) on a hexagonal grid.



(b)

FIGURE 9. Labeling conventions for hexagonal grid. (a) Standard; and (b) Alternative.

2(b). Another choice of G for $P = 2$ is

$$G(\mathbf{v}, \mathbf{d}, \lambda_1, \lambda_2) = \|\mathbf{v} - \mathbf{d}\|^2 + \lambda_1(\|\mathbf{D}_1\mathbf{v}\|^2 + \|\mathbf{D}_2\mathbf{v}\|^2 + \|\mathbf{D}_3\mathbf{v}\|^2) + \lambda_2(\|\mathbf{L}_1\mathbf{v}\|^2 + \|\mathbf{L}_2\mathbf{v}\|^2 + \|\mathbf{L}_3\mathbf{v}\|^2) \quad (70)$$

where

$$\mathbf{L}_1 := -\mathbf{D}_1^T \mathbf{D}_1, \quad \mathbf{L}_2 := -\mathbf{D}_2^T \mathbf{D}_2, \quad \mathbf{L}_3 := -\mathbf{D}_3^T \mathbf{D}_3. \quad (71)$$

The solution is given by

$$\mathbf{v} - \mathbf{d} - \lambda_1 \mathbf{L}\mathbf{v} + \lambda_2(\mathbf{L}_1^T \mathbf{L}_1 + \mathbf{L}_2^T \mathbf{L}_2 + \mathbf{L}_3^T \mathbf{L}_3)\mathbf{v} = \mathbf{0}. \quad (72)$$

Note that the last term $\mathbf{L}_1^T \mathbf{L}_1 + \mathbf{L}_2^T \mathbf{L}_2 + \mathbf{L}_3^T \mathbf{L}_3$ in eqn (72) is not $\mathbf{L}\mathbf{v}$ and it reads (compare with eqn (69))

$$v_{i-2,j} + v_{i+2,j} + v_{i,j-2} + v_{i,j+2} + v_{i-2,j+2} + v_{i+2,j-2} - 4(v_{i-1,j-1} + v_{i+1,j} + v_{i,j+1} + v_{i,j+1} + v_{i-1,j+1} + v_{i+1,j-1}) + 18v_{i,j} \quad (73)$$

which is a rather crude approximation of $\mathbf{L}^2\mathbf{v}$. The network given in Figure 1 and hence in Figure 3 minimizes eqn (70) with $\lambda_1 = 0$, $\lambda_2 > 0$.

3. $P = 3$. A possible choice of G will be

$$G(\mathbf{v}, \mathbf{d}, \lambda_1, \lambda_2, \lambda_3) = \|\mathbf{v} - \mathbf{d}\|^2 + \lambda_1(\|\mathbf{D}_1\mathbf{v}\|^2 + \|\mathbf{D}_2\mathbf{v}\|^2 + \|\mathbf{D}_3\mathbf{v}\|^2) + \lambda_2\|\mathbf{L}\mathbf{v}\|^2 + \lambda_3(\|\mathbf{D}_1\mathbf{L}\mathbf{v}\|^2 + \|\mathbf{D}_2\mathbf{L}\mathbf{v}\|^2 + \|\mathbf{D}_3\mathbf{L}\mathbf{v}\|^2). \quad (74)$$

Note that the third term corresponds to one of the penalty terms considered in Poggio et al. (1985) for the continuous two-dimensional problem. The solution is given by

$$\mathbf{v} - \mathbf{d} - \lambda_1 \mathbf{L}\mathbf{v} + \lambda_2 \mathbf{L}^2\mathbf{v} - \lambda_3 \mathbf{L}^3\mathbf{v} = \mathbf{0}. \quad (75)$$

We will stop here and formalize the argument in the following:

Fact 3. Consider the minimization problem on a hexagonal array:

$$G(\mathbf{v}, \mathbf{d}, \lambda_1, \dots, \lambda_p) = \|\mathbf{v} - \mathbf{d}\|^2 + \sum_{r=1}^p \begin{cases} \lambda_r \|\mathbf{L}^{r/2}\mathbf{v}\|^2 & r: \text{even} \\ \lambda_r (\|\mathbf{D}_1 \mathbf{L}^{r-1/2}\mathbf{v}\|^2 + \|\mathbf{D}_2 \mathbf{L}^{r-1/2}\mathbf{v}\|^2 + \|\mathbf{D}_3 \mathbf{L}^{r-1/2}\mathbf{v}\|^2) & r: \text{odd} \end{cases} \quad (76)$$

where \mathbf{L} , \mathbf{D}_1 , \mathbf{D}_2 and \mathbf{D}_3 are defined by eqns (65), (61), (62) and (63), respectively. Then the statements of Fact 1 are valid.

4. APPLICATION: THE SCE FILTER

Specializing Fact 1 to $P = 2$, one has a rather interesting application.

Fact 4. Consider the double-layer network given in Figure 10.

1. The first layer solves the first order regularization with $\lambda_1 = g_{s1}/g_{m1}$, $d_k = (1/g_{m1})u_k$, while the second layer solves the second order regularization with $\lambda_2 = (g_{s1}g_{s2})/(g_{m1}g_{m2})$, $\lambda_1 = (g_{m1}g_{s2} +$

$g_{m2}g_{s1})/(g_{m1}g_{m2})$, $d_k = (T_1/(g_{m1}g_{m2}))u_k$, simultaneously.

2. Let

$$x_k = v_k^1 - v_k^2. \quad (77)$$

Then x_k enhances contrasts after smoothing (with appropriate parameters).

3. Consider the uniform input $u_k \equiv u$ for all k . If

$$g_{m2} = T_1 \quad (78)$$

then

$$x_k \equiv 0 \quad \text{for all } k. \quad (79)$$

REMARKS.

1. Figure 11 shows the one-dimensional responses of v_k^1 , v_k^2 and x_k to the input

$$u_k = \begin{cases} 5 \mu\text{A} & 29 \leq k \leq 31 \\ 0 & \text{elsewhere} \end{cases} \quad (80)$$

with

$$1/g_{m1} = 1/g_{m2} = 500 \text{ k}\Omega, \quad 1/g_{s1} = 120 \text{ k}\Omega, \\ 1/g_{s2} = 20 \text{ k}\Omega, \quad T_1 = 2 \times 10^{-6} \text{ Siemens}. \quad (81)$$

Observe that the second layer response v_k^2 alone already accomplishes the second order regularization without negative conductance. Note also that since the input (80) is a narrow "slit" located at the center, the response x_k (a) smooths the input and then (b) enhances contrasts because of the antagonistic surround. In order to see these capabilities more clearly, let us consider the input given by Figure 12(a) which is a rectangular "image" given by

$$u_k = \begin{cases} 4 \mu\text{A} & 24 \leq k \leq 38 \\ 0 & \text{elsewhere.} \end{cases} \quad (82)$$

Figure 12(b) shows the filter response x_k . Figure 12(c) is the input u_k corrupted by a Gaussian noise n_k with $3\sigma = 1 \mu\text{A}$, i.e.,

$$u'_k = u_k + n_k. \quad (83)$$

Figures 12(d) and (e) give the filter responses. Figure 12(f) gives the response x_k to the noisy input (83) when all the circuit parameters are perturbed according to the Gaussian distribution around the nominal values with $3\sigma = 20\%$. When the network is implemented by an analog CMOS VLSI, the resistance values naturally deviate from the nominal values. These data suggest that the filter is capable of achieving Smoothing-Contrast Enhancing (SCE) with reasonable robustness against parameter variations.

2. In engineering terms, this network can be regarded as a noncausal¹ infinite impulse response (IIR) im-

¹ Non-causal is referred to the fact that the voltage at a particular node depends on the node voltages "to the right" as well as on those "to the left."

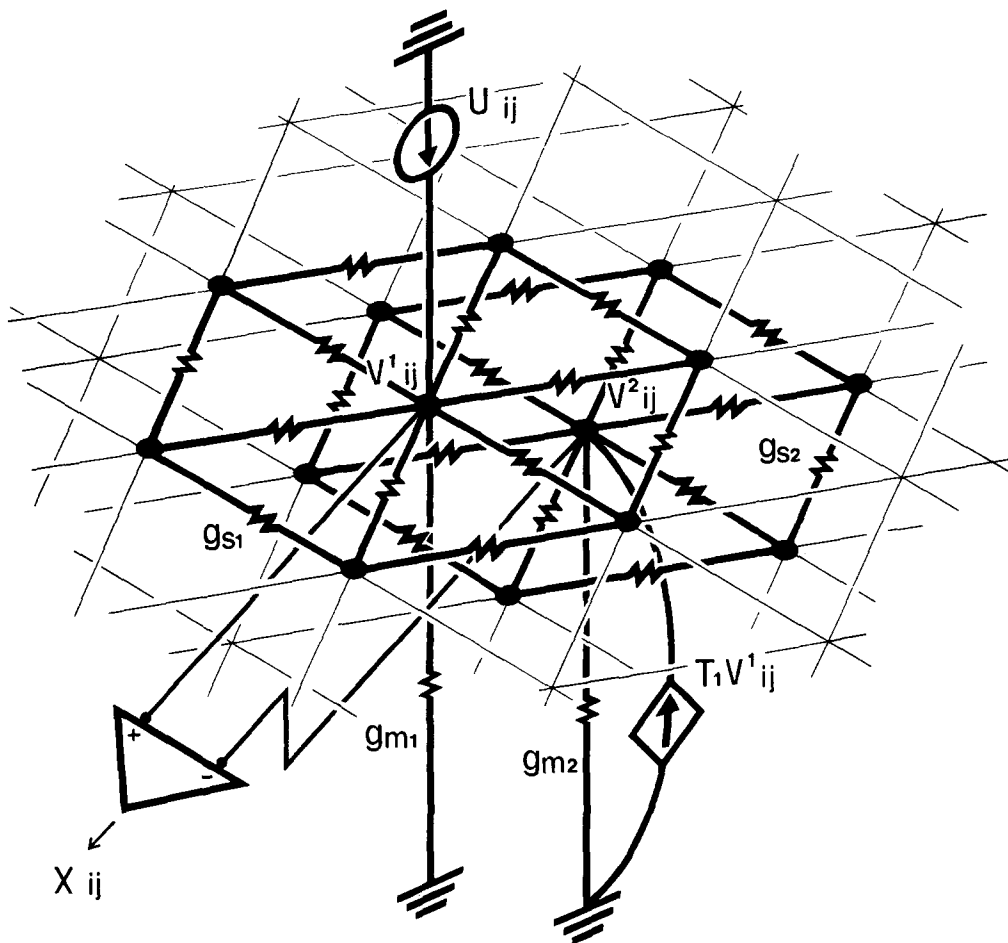


FIGURE 10. A double-layer network.

plementation of a $\nabla^2 G$ -like filter. Speaking roughly, our filter output x is $(L^{-1} - L^{-2})u$ where L is as defined by eqn (5) (see Remark after Fact 1). We are avoiding the term "edge detection" simply because a zero crossing of $\nabla^2 G$ is not necessarily an edge (Clark, 1989). Note, however, that in the particular situation given in Figure 12(f), our SCE filter correctly identifies the two edges against noise and parameter variations, if one checks the zero crossings.

3. In order to prove statement 3 of Fact 4, note that the input being uniform implies that no current can flow through g_{s1} , and hence, $v_k^1 \equiv u/g_{m1}$. Similarly, $v_k^2 \equiv (T_1/g_{m1}g_{m2})u$ which yields $v_k^1 - v_k^2 = u/g_{m1} - (T_1/g_{m1}g_{m2})u \equiv 0$. Thus, eqn (78) implies eqn (79). This means that if eqn (78) holds, then x_k does not respond to the "DC component," namely, x_k responds only to intensity differences and is insensitive to absolute values. This is important from the information processing viewpoint.
4. That the voltage controlled current source $T_1 v^1$ is a unilateral element is important. Namely, while the first layer voltage v^1 does affect the second layer via $T_1 v^1$, the second layer voltage v^2 has no effect on the first layer. Thus, if $T_1 v_k^1$ were replaced with a passive

resistor (a bilateral element), then $v_k^1 > v_k^2$ always and hence eqn (79) could never be satisfied. It is also clear that there would be no antagonistic surround.

5. The simplicity of the architecture naturally implies the simplicity of the circuitry. Figure 13 shows a possible circuit block diagram realizing a unit "cell." An image is directly shined onto an array of phototransistors through a lens. The light which hits the base of the phototransistor induces a current which is converted into a voltage so that the input circuit is a Thevenin equivalent of the input circuit of Figure 5. A similar circuit is used for the second layer input. The two triangles together with switches are for the input and output data readout. Although details on the chip implementation will be reported elsewhere, Table 1 shows several quantitative comparisons between the Gaussian chip reported in Kobayashi et al. (1990, 1991) and the SCE chip proposed here.
6. After this work was completed, K. Uchimura of NTT VLSI Laboratory brought our attention to Yasuda et al. (1971), where architecture consisting of two layers of resistive network was proposed and implemented by discrete components 20 years ago. An

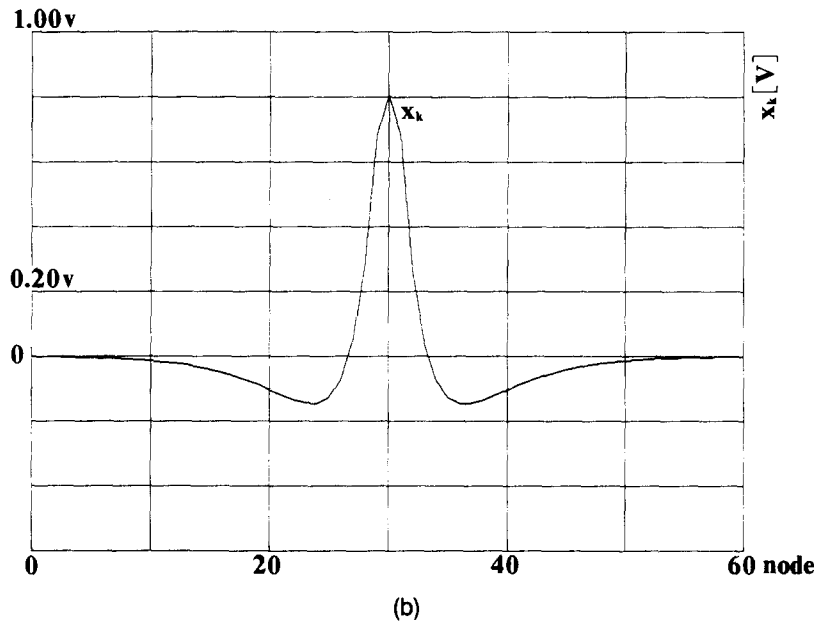
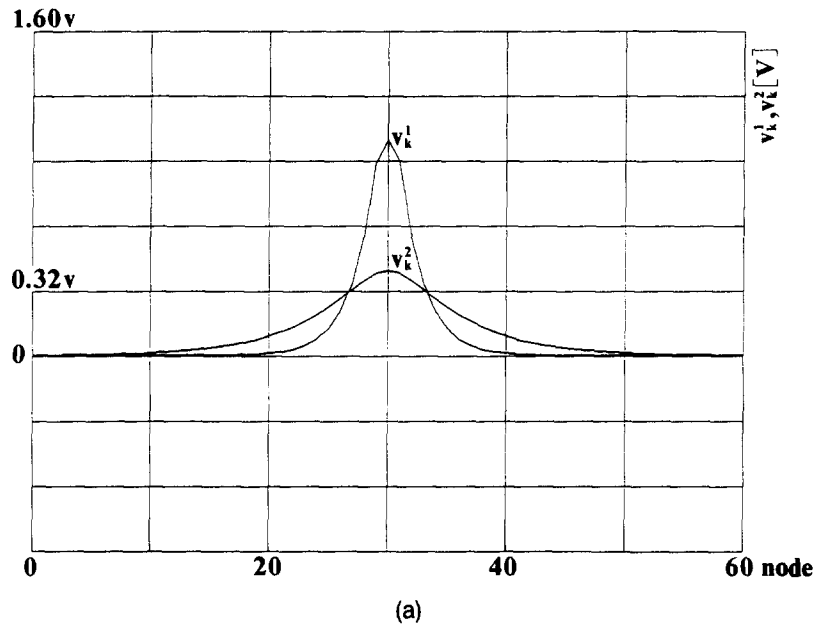


FIGURE 11. Responses of the double-layer network to a “narrow slit” located at the center;

(a) v_k^1 and v_k^2 (b) x_k .

$$u_k = \begin{cases} 5 \mu\text{A} & 29 \leq k \leq 31 \\ 0 & \text{elsewhere.} \end{cases}$$

input circuit was implemented by an array (703) of silicon solar cells and the current induced by an image was fed into the two resistive networks. There is a **crucial** difference between the architecture considered in Yasuda et al. (1971) and the architecture proposed in this paper. In the former, the two layers receive exactly the **same** input current and there is no voltage controlled current source. This is done by simply sharing the input wire. Therefore, both layers perform the first order regularization. The network

outputs the difference between the first and the second layer voltages. In order for the output to have a meaningful contrast enhancement effect, the second layer resistance value must be significantly smaller than that of the first layer. In fact, in Yasuda et al. (1971), the ratio is 68 k Ω :1 k Ω . The latter dissipates a great amount of power and yet antagonistic surround of a measured response is barely discernible. Recall that in our architecture, the ratio is 120 k Ω :20 k Ω (see eqn (81)) and yet x_k has a significant

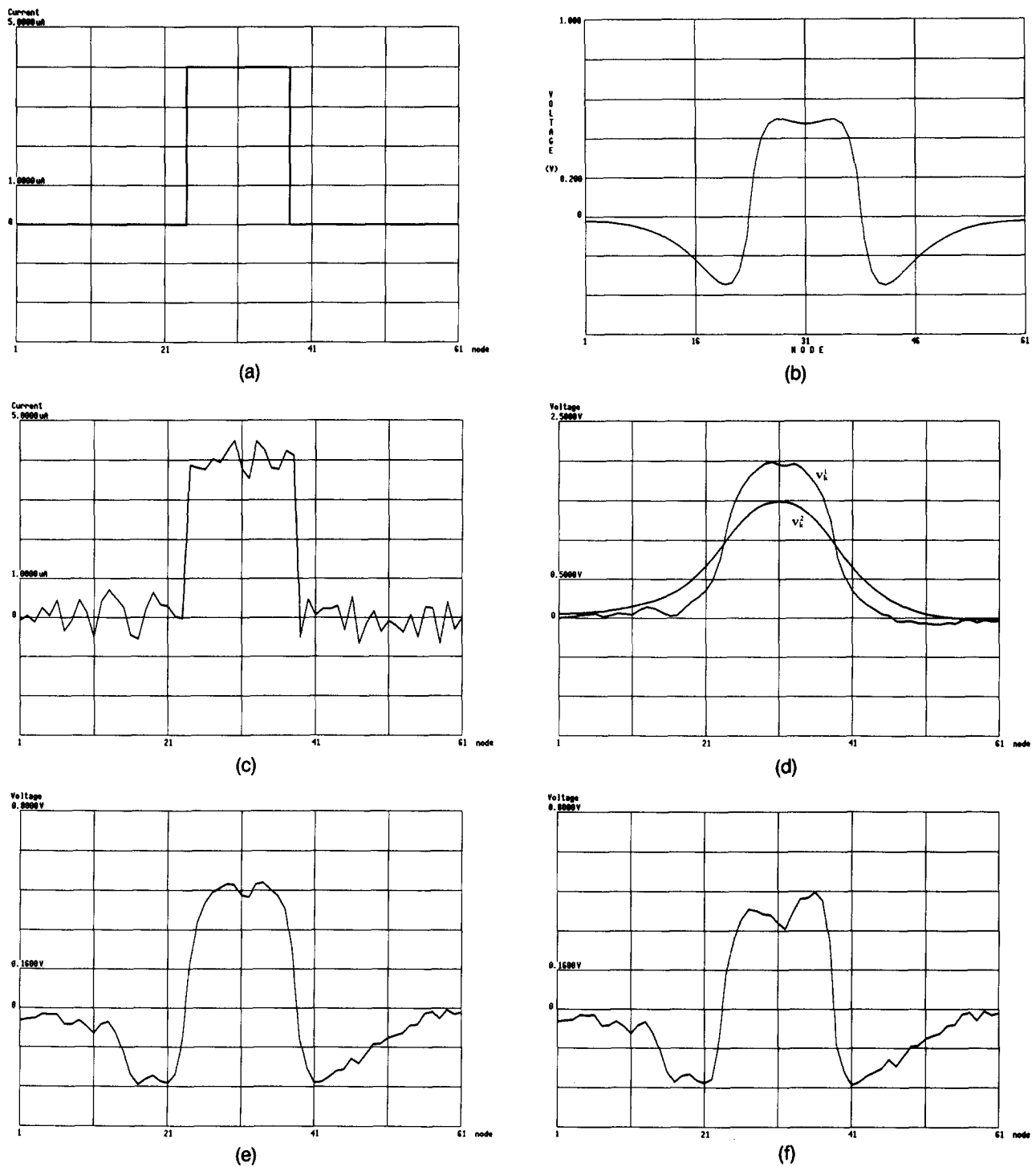


FIGURE 12. Responses to noisy input. (a) Noiseless input where

$$u'_k = \begin{cases} 4 \mu\text{A} & 24 \leq k \leq 38 \\ 0 & \text{elsewhere;} \end{cases}$$

(b) Responses to (a); (c) Input is corrupted by a white Gaussian noise with $3\sigma = 1 \mu\text{A}$; (d) Response v_1 and v_2 ; (e) Response x_k ; and (f) Response x_k when all the circuit parameters are perturbed by Gaussian around the nominal values with $3\sigma = 20\%$.

*contrast enhancement effect. This is due to the voltage controlled current source $T_1 v_k$ which enables the second layer to perform the **second order regularization** rather than the first order regularization. We would like to point out that our network can*

perform contrast enhancement even with $g_{s1} = g_{s2}$. Figure 14 gives the response x_k to

$$u_k = \begin{cases} 5 \mu\text{A} & 29 \leq k \leq 31 \\ 0 & \text{elsewhere} \end{cases} \quad (84)$$

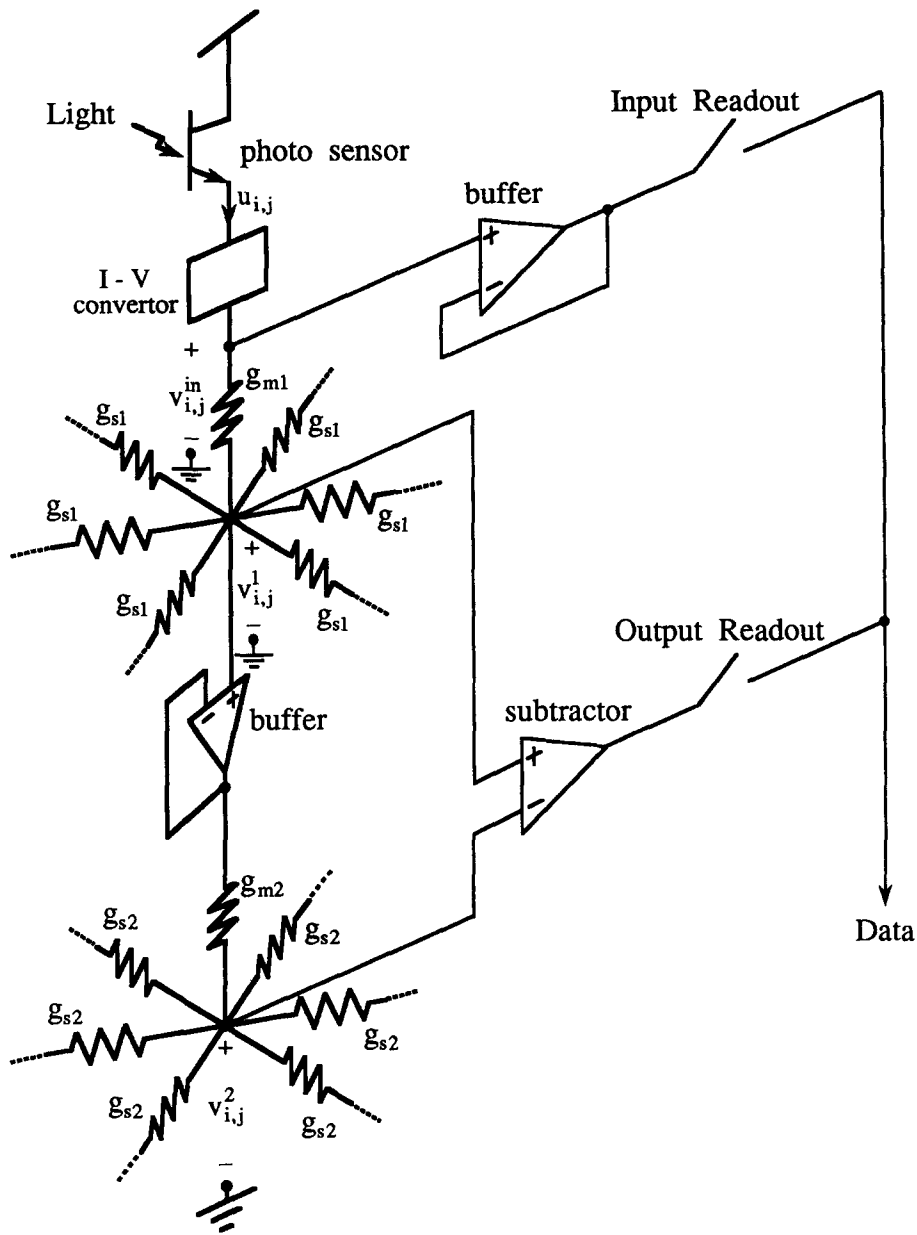


FIGURE 13. A schematic block diagram for a unit cell of the SCE filter.

where $1/g_{s_1} = 1/g_{s_2} = 120 \text{ k}\Omega$ and other parameters are as in eqn (81). If one interprets the first order regularization as a single convolution, then the second layer voltage is a result of taking two successive convolutions thus obtaining a radical broadening of the impulse response.

7. The network reported in (Mead, 1989; Mead & Mahowald, 1988) is single-layered, and computes, in our notation, $u_k - v_k$. Namely, the network outputs the difference between the input and its "first order regularized" signal.

As was remarked in Section 2, the spatial dynamics of the double-layer network in Figure 10 cannot have complex eigenvalues. We will show that for the network given in Figure 15, which is a slight modification of Figure 10, the F-matrix (see eqn (39)) admits complex

eigenvalues. As will be described in Section 4, the network of Figure 15 is the model proposed by one of the authors for lower vertebrate retina.

Fact 5. Consider the network of Figure 16 where $g_{m_1}, g_{m_2}, g_{s_1}, g_{s_2} > 0$, and

$$T_1 T_2 < 0. \tag{85}$$

Then

1. The network is temporally stable in the sense of Fact 1.
2. At an equilibrium, the second layer solves the second order regularization with

$$\lambda_2 = \frac{g_{s_1} g_{s_2}}{g_{m_1} g_{m_2} - T_1 T_2}, \quad \lambda_1 = \frac{g_{m_1} g_{s_2} + g_{m_2} g_{s_1}}{g_{m_1} g_{m_2} - T_1 T_2},$$

$$d_k = \frac{T_1}{g_{m_1} g_{m_2} - T_1 T_2} u_k. \tag{86}$$

TABLE 1
Comparison Between Gaussian Chip and SCE Chip

	Gaussian Chip	SCE Chip
unit cell size	200 μm \times 170 μm	160 μm \times 138 μm
transistor count	50/unit cell	50/unit cell
power dissipation	1.1 mW/unit cell	0.1 mW/unit cell
quality of smoothing	\odot	\circ

3. The first layer solves the first order regularization with

$$\lambda_1 = \frac{g_{s1}}{g_{m1}}, \quad d_k = \frac{1}{g_{m1}} (u_k + T_2 v_k^2), \quad (87)$$

where v_k^2 is the solution for (2).

4. The network is spatially stable in the sense of Matsumoto et al. (1991, 1992).
5. If

$$\left(\frac{g_{m1}}{g_{s1}} - \frac{g_{m2}}{g_{s2}} \right)^2 + 4 \frac{T_1 T_2}{g_{s1} g_{s2}} < 0 \quad (88)$$

then the eigenvalues of the F-matrix are two sets of *complex conjugate* pairs off the unit circle.

REMARKS. (a) *The only difference between Figure 15 and Figure 10 is the presence of the feedback $T_2 v_k^2$ from the second layer to the first layer.* (b) *It follows from eqn (86) that λ_2 can be controlled by $T_1 T_2$ without changing the ratio λ_1 / λ_2 .*

Proof. (a) We will prove the one-dimensional case. Because of the feedback $T_2 v^2$, the first layer is **not** independent of the second layer. Letting C^1 (resp. C^2) be the parasitic capacitance matrix of the first (resp. second) layer, one has the dynamics of the network

$$C^1 \frac{dv^1}{dt} = (g_{s1} \mathbf{L} - g_{m1} \mathbf{1}) v^1 + T_2 v^2 + \mathbf{u} \quad (89)$$

$$C^2 \frac{dv^2}{dt} = (g_{s2} \mathbf{L} - g_{m2} \mathbf{1}) v^2 + T_1 v^1 \quad (90)$$

where $\mathbf{1}$ is the identity matrix. Since $T_1 T_2 < 0$ (see eqn (85)), assume, without loss of generality, that

$$T_1 > 0, \quad T_2 = -|T_2|. \quad (91)$$

Multiply eqn (90) by $|T_2|/T_1$ to obtain

$$\frac{|T_2|}{T_1} C^2 \frac{dv^2}{dt} = \frac{|T_2|}{T_1} (g_{s2} \mathbf{L} - g_{m2} \mathbf{1}) v^2 + |T_2| v^1 \quad (92)$$

so that eqns (89) and (92) can be recast as

$$\mathbf{C} \frac{d\mathbf{v}}{dt} = (\mathbf{A} + \mathbf{B}) \mathbf{v} + \mathbf{D} \mathbf{u} \quad (93)$$

where $\mathbf{v} = (v^1, v^2)^T$, and

$$\mathbf{A} = \begin{bmatrix} g_{s1} \mathbf{L} - g_{m1} \mathbf{1} & \mathbf{0} \\ \mathbf{0} & \frac{|T_2|}{T_1} (g_{s2} \mathbf{L} - g_{m2} \mathbf{1}) \end{bmatrix} \quad (94)$$

$$\mathbf{C} = \begin{bmatrix} C^1 & \mathbf{0} \\ \mathbf{0} & \frac{|T_2|}{T_1} C^2 \end{bmatrix},$$

$$\mathbf{B} = \begin{bmatrix} \mathbf{0} & -|T_2| \mathbf{1} \\ |T_2| \mathbf{1} & \mathbf{0} \end{bmatrix}, \quad \mathbf{D} = \begin{bmatrix} \mathbf{1} \\ \mathbf{0} \end{bmatrix}. \quad (95)$$

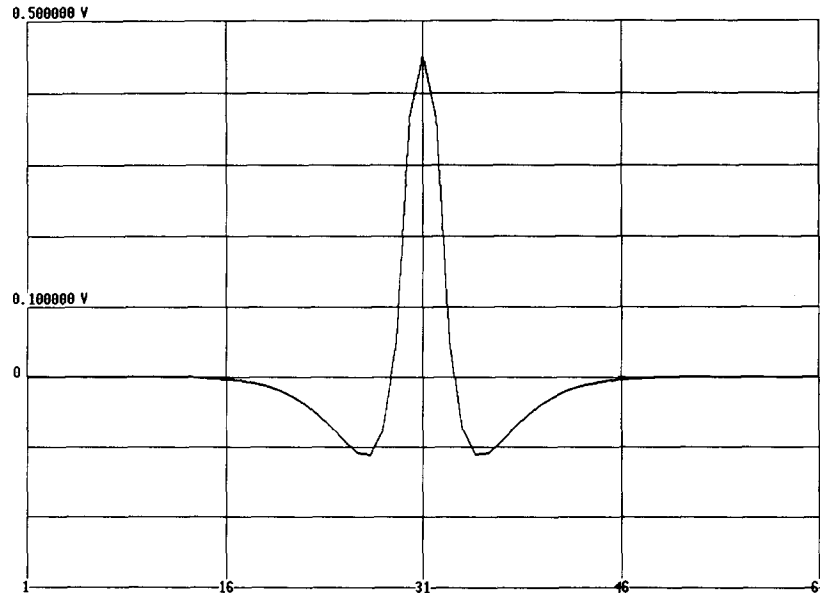


FIGURE 14. Second order regularization enables contrast enhancement even with $1/g_{s1} = 1/g_{s2} = 120 \text{ k}\Omega$ where other parameters are the same as in eqn (81).

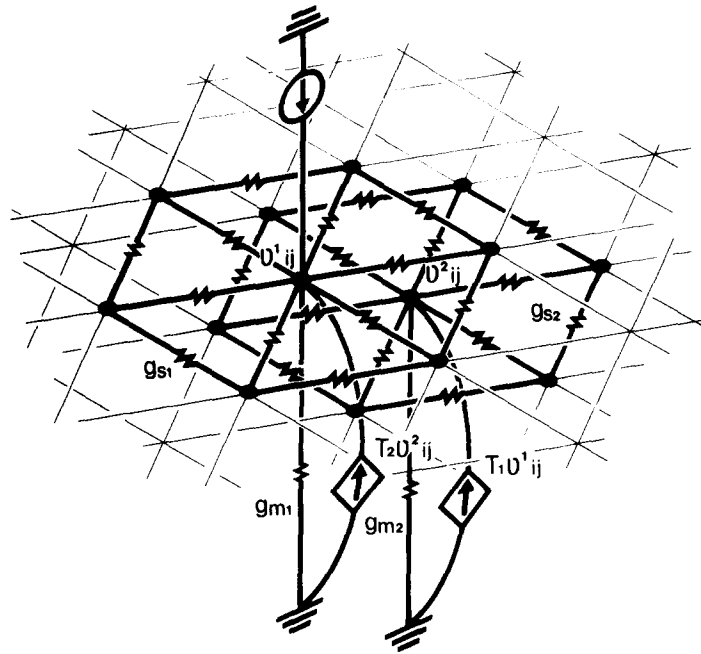


FIGURE 15. A double-layer network with feedback.

Since \mathbf{B} is not symmetric, this network is **not** reciprocal (Matsumoto, 1976) and hence, the cocontent (Matsumoto et al., 1992; Poggio et al., 1985) is *undefined*, i.e., the dynamics is not the gradient of a scalar function. The stability, however, is almost trivial because \mathbf{L} being positive definite implies the negative definiteness of \mathbf{A} and

$$\frac{d}{dt} \left(\frac{1}{2} \mathbf{v}^T \mathbf{C} \mathbf{v} \right) = \mathbf{v}^T (\mathbf{A} + \mathbf{B}) \mathbf{v} = \mathbf{v}^T \mathbf{A} \mathbf{v} < 0 \quad (96)$$

where $\mathbf{v}^T \mathbf{B} \mathbf{v} = 0$ was used. Since \mathbf{C} is positive definite, $\mathbf{A} + \mathbf{B}$ is stable. (b) and (c) can be proven in a manner

similar to the proof of Fact 1. (d) Because of the feedback $T_2 \mathbf{v}_2$, spatial stability is nontrivial. Note that at an equilibrium, v_k^2 satisfies

$$\begin{aligned} &-(g_{m1}g_{m2} - T_1T_2 + 6g_{s1}g_{s2} + 2g_{m1}g_{s2} + 2g_{m2}g_{s2})v_k^2 \\ &+ (4g_{s1}g_{s2} + g_{m1}g_{s2} + g_{m2}g_{s1})(v_{k-1}^2 + v_{k+1}^2) \\ &- g_{s1}g_{s2}(v_{k-2}^2 + v_{k+2}^2) + T_1u_k = 0. \end{aligned} \quad (97)$$

Putting

$$\begin{aligned} g_0 &:= g_{m1}g_{m2} - T_1T_2, \\ g_1 &:= 4g_{s1}g_{s2} + g_{m1}g_{s2} + g_{m2}g_{s1}, \quad g_2 := -g_{s1}g_{s2}, \end{aligned} \quad (98)$$

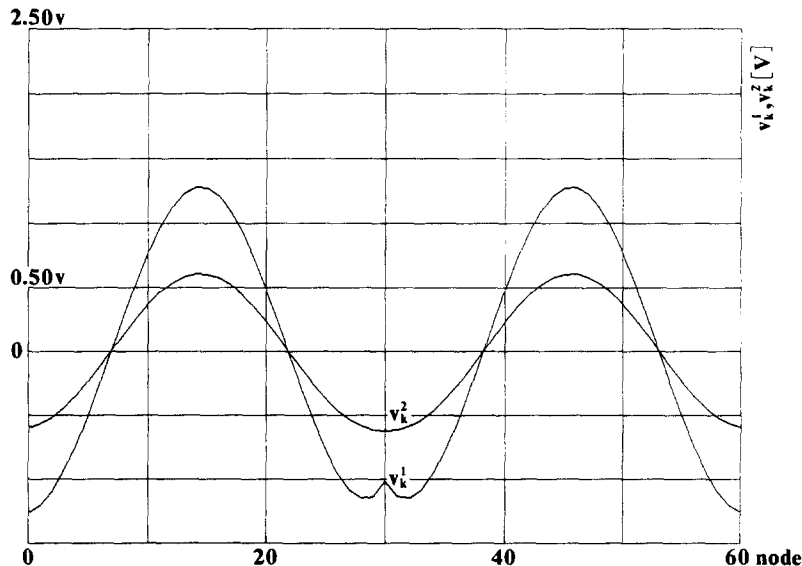


FIGURE 16. Unstable spatial responses.

one sees that eqn (97) reads

$$-(g_0 + 2g_1 + 2g_2)v_k^2 + g_1(v_{k-1}^2 + v_{k+1}^2) + g_2(v_{k-2}^2 + v_{k+2}^2) + T_1 u_k = 0. \quad (99)$$

This difference equation can be recast as $\mathbf{x}_{k+1} = \mathbf{F}\mathbf{x}_k + \mathbf{y}_k$ where

$$\mathbf{F} = \begin{bmatrix} 0 & 1 & 0 & 0 \\ 0 & 0 & 1 & 0 \\ 0 & 0 & 0 & 1 \\ -1 & -g_1/g_2 & (g_0 + 2g_1 + 2g_2)/g_2 & -g_1/g_2 \end{bmatrix}. \quad (100)$$

It is shown in Matsumoto et al. (1992) that dynamics is stable if \mathbf{F} is hyperbolic, i.e., it has no eigenvalues on the unit circle. It follows from Proposition 3.4 of Matsumoto et al. (1991, 1992) that eqn (100) is stable iff $\sigma_+(g_0, g_1, g_2) < 0$

where

$$\sigma_+(g_0, g_1, g_2) = \begin{cases} -g_0 - 2g_1 + 2|g_1| & \text{when } g_2 > 0 \text{ or } g_2 < 0 \text{ and } |g_1/g_2| \geq 4 \\ -g_0 - 2g_1 - 4g_2 - g_1^2/(4g_2) & \text{when } g_2 < 0 \text{ and } |g_1/g_2| \leq 4. \end{cases} \quad (101)$$

It follows from eqn (98) that $g_2 < 0, g_1 > 0$ and $|g_1/g_2| > 4$ so that $\sigma_+(g_0, g_1, g_2) = -g_0 = -(g_{m_1}g_{m_2} - T_1T_2)$. Therefore, the network is spatially stable if

$$g_{m_1}g_{m_2} - T_1T_2 > 0. \quad (102)$$

Our assumption that $T_1T_2 < 0$ implies spatial stability. (e) It follows from eqn (46) that if eqn (88) is satisfied, then the eigenvalues are complex as stated. ■

REMARKS. (a) Figure 16 shows typical impulse responses of v_k^1 and v_k^2 when eqn (102) is violated, which is highly undesirable. Note that in the present network, eqn (102) is equivalent to the fact that $\lambda_1, \lambda_2 > 0$. (b) Of course, if $T_2 = 0$, then eqn (102) is trivially satisfied and hence, the network of Figure 10 is spatially stable.

5. WIRING COMPLEXITY

The term ‘‘wiring complexity’’ is not our invention. It is repeatedly emphasized in (Mead, 1989, p. 7, p. 116, pp. 276–277) as the **single most important** issue. It is indeed critical for implementing vision chips because although each computing unit has relatively simple circuitry, there are thousands of computing units placed regularly so that the routing can be extremely difficult when the network architecture demands complicated interconnections among computing units.

As was shown in Figure 3, complexity of the wiring

becomes serious when one wants to solve regularization problems in two dimensions, and yet the network is only a crude approximation to the biharmonic operator (see eqn (72)). If one wants to implement eqn (68), the wiring gets even more serious. Let us look at, for instance, Figure 17 which implements eqn (68) (g_0 and input are not shown) provided that

$$g_1:g_2:\tilde{g}_2 = 10 + \frac{\lambda_1}{\lambda_2}:-2:-1 \quad (103)$$

because the KCL reads

$$\begin{aligned} &-(g_0 + 6g_1 + 6g_2 + 6\tilde{g}_2)v_{i,j} + g_1(v_{i-1,j} + v_{i+1,j} \\ &+ v_{i,j-1} + v_{i,j+1} + v_{i-1,j+1} + v_{i+1,j-1}) \\ &+ g_2(v_{i-2,j} + v_{i+2,j} + v_{i,j-2} + v_{i,j+2} + v_{i-2,j+2} + v_{i+2,j-2}) \\ &+ \tilde{g}_2(v_{i-1,j-1} + v_{i+1,j+1} + v_{i-1,j+2} + v_{i+1,j-2} \\ &+ v_{i-2,j+1} + v_{i+1,j-1}) + u_{i,j} = 0 \end{aligned} \quad (104)$$

where u_{ij} is the input current source. Thus, the network of Figure 1 corresponds to $\tilde{g}_2 = 0$ in Figure 18. Since Fact 2 claims that the layered network of Figure 5 with only immediate neighbor connections, there must be a significant reduction of wiring complexity. This section tries to quantify the wiring complexity.

Let us first note that there are basically three categories in vision chip wiring:

- Class 1:** Conductance interconnections between unit cells.
- Class 2:** Power supply lines and bias voltage lines.
- Class 3:** Data lines and address lines for data readout.

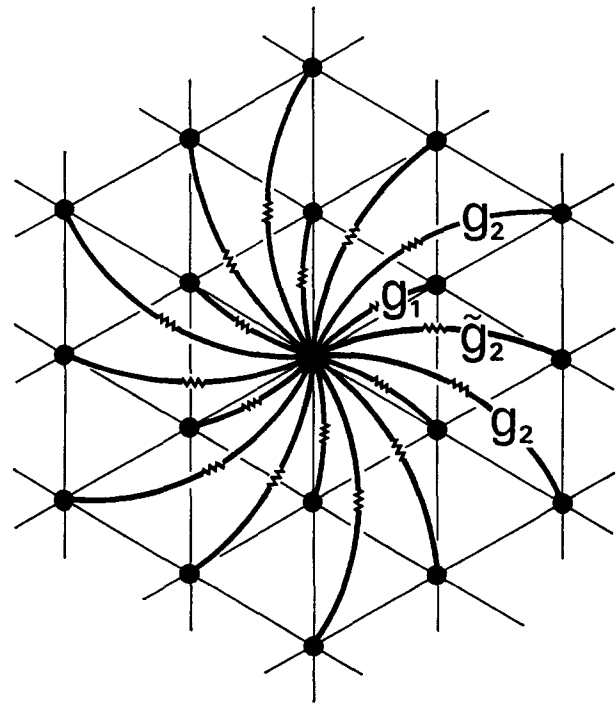


FIGURE 17. A network implementing L^2 . g_0 and input are not shown.

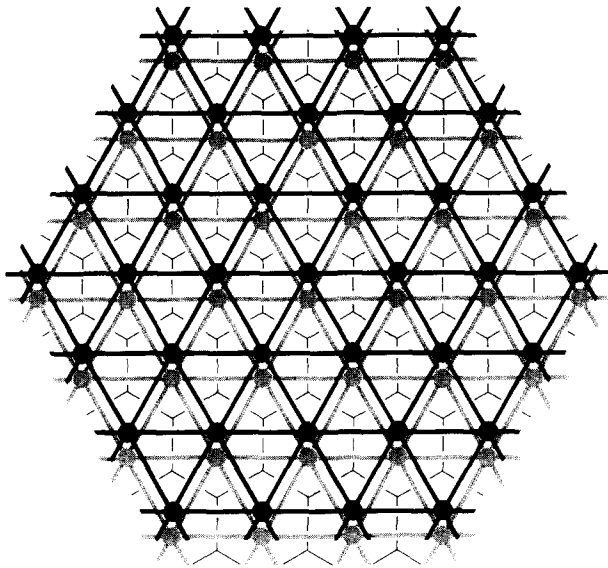


FIGURE 18. Wiring complexity of the layered network with $P = 2$ amounts to 6. A hexagon stands for a unit cell.

Even though these are not completely independent of each other, we will pay particular attention to Class 1 because it is the dominant one and critically dependent on the architecture of the signal processing part. Class 2 depends much more heavily on circuit design than the architecture. Class 3 essentially depends on the data readout mechanism.

Since a precise technical definition of wiring complexity is not given in Mead (1989), we will try to give a reasonable one here. Naturally we do not claim this is the best, nor only definition. In order to quantify wiring complexity, several simplifications are necessary. As far as wiring complexity is concerned, the following assumption will be made.

ASSUMPTION. *The lateral conductances are regarded as pure wires, while the vertical conductances as well as the input circuit are regarded as a "unit cell."*

REMARK. *Conductances g_1 and g_2 in Figure 1 will be regarded as pure wires whereas g_0 and the input circuit are regarded as a unit cell. Similarly, g_{s_1} and g_{s_2} in Figure 10 are regarded as pure wires whereas g_{m_1} , g_{m_2} and the input circuit constitute a unit cell.*

A natural question arises. Doesn't the unit cell of a multilayered network need more chip area than that of a single layered network? Not necessarily. Let us compare, for instance, Figure 4 and Figure 10. First note that in actual implementations, $\frac{1}{2}$ of each lateral resistor $1/g_r$ or $1/g_s$ is realized in each unit cell area. Second, since g_2 in Figure 4 is negative, it demands more transistors. In Kobayashi et al. (1990, 1991), g_2 necessitates a transconductance amplifier and six transistors per node. In Figure 14, the voltage controlled current source is realized by a differential amplifier to-

gether with g_{m_2} and hence six transistors are enough per node. Thus the unit cell area of a layered network would not be any larger. Hence the wiring complexity of a chip is the complexity of wiring among unit cells. We assume, therefore, that the unit cell area is normalized to 1×1 .

DEFINITION. *The wiring complexity of a vision chip is defined as the number of wires which cross a unit cell.*

REMARKS. (a) *The unit cell defined above corresponds to a pixel.* (b) *For the wiring complexity, one has to count not only the wires connecting a particular unit with another unit but also those which pass through a unit cell for the purpose of connecting other cells together.* (c) *If the unit cell is normalized to 1×1 , our definition of wiring complexity means the wire length. Observe that for a chip implementation, a wire which comes into a unit cell area contributes to the same complexity whether or not there is an electrical contact at the unit cell because one simply places a "via" (hole) if there is an electrical contact.*

Fact 5. *Consider the layered network of Figure 5 on a hexagonal grid. If the number of layers is P , then*

$$\text{wiring complexity} = 3P. \quad (105)$$

Proof. Since each layer has only immediate neighbor connections, three wires cross each unit cell represented by a hexagon. ■

Figure 18 shows the case with $P = 2$. As for a single-layer network with general P on a hexagonal grid, the wiring complexity formula itself gets complicated. We will give formulas up to $P = 3$ which is enough for the present purpose.

Fact 6. (a) *For the single-layer network which implements eqn (64) ($P = 1$),*

$$\text{wiring complexity} = 3. \quad (106)$$

(b) *For the single-layer network of Figure 17 which implements eqn (68) ($P = 2$),*

$$\text{wiring complexity} = 15. \quad (107)$$

(c) *For the single-layer network of Figure 17 with $\tilde{g}_2 = 0$, which implements eqn (72) ($P = 2$),*

$$\text{wiring complexity} = 9. \quad (108)$$

(d) *For the single-layer network of Figure 19 which implements eqn (75) ($P = 3$),*

$$\text{wiring complexity} = 33. \quad (109)$$

Proof. For $P = 1$, the single-layer network and the "multilayer network" coincide. Consider the network of Figure 17 which implements eqn (68). There are three classes of wires which cross a unit cell represented by a hexagon:

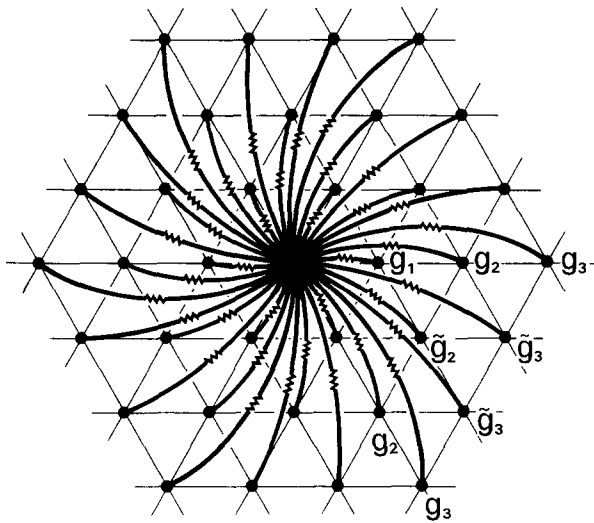


FIGURE 19. A network solving the problem with $P = 3$.

1. The g_1 -connections which give rise to three wires crossing a unit cell (Figure 20). The g_2 -connections demand six wires not three because, in addition to the three wires which connect each unit cell with its second neighbors, there is another set of three wires connecting between the neighboring nodes.
2. In order to see the complexity of the g_2 -connections, let us look at Figure 21. In order to avoid an obvious technical difficulty in drawing the figure, four different textures are used for wires. Where a circle is placed with a particular texture, there is an electrical contact by a wire with that particular texture.
3. The \tilde{g}_2 -connections also demand six wires. In order to demonstrate this, let us look at Figure 3. First, note that the wires drawn in this figure are not present in Figure 21. For instance, there are no “horizontal” connections in Figure 22, while “vertical”

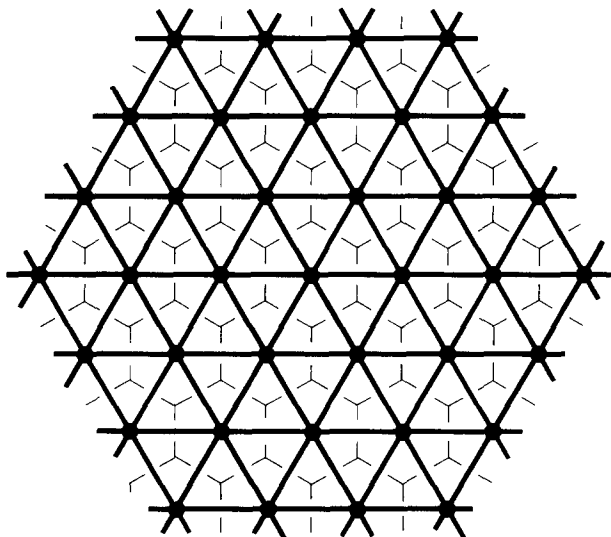


FIGURE 20. Wiring complexity of the g_1 -connections contributes 3.

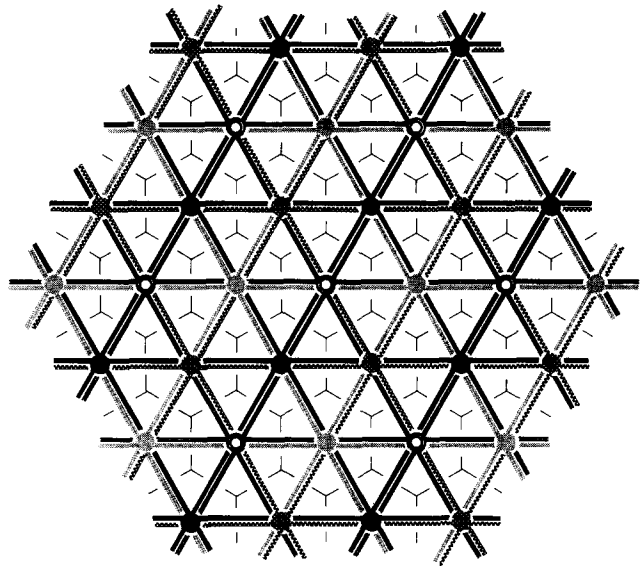


FIGURE 21. Wiring complexity of the g_2 -connections is 6. Three wires connect a cell with its second nearest neighbor while another three wires pass through each cell.

connections are present which are not present in Figure 21. Thus, in addition to the three wires which cross a unit cell “in the middle,” there are six other wires passing through the “boundary” of a unit cell represented by a hexagon. Since a wire must pass through somewhere, by an appropriate “splitting,” one sees that the complexity contribution from these wires is three.

Therefore, $3 + 6 + 6 = 15$ wires contribute to the complexity which is eqn (107). If $\tilde{g}_2 = 0$, then one has nine wires which is eqn (108). Using a similar argument, one can show that the g_3 -connections and the \tilde{g}_3 connections of Figure 21 demand 18 wires which must be added to 15 and hence, the complexity is 33. ■

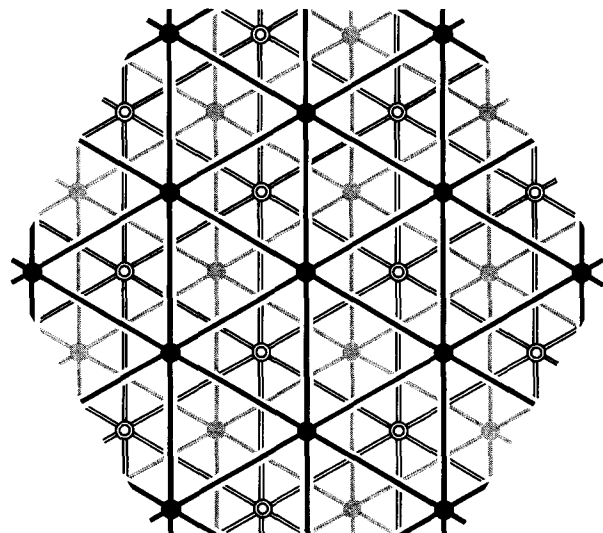


FIGURE 22. The \tilde{g}_2 -connections contribute another 6.

Reduction of the wiring complexity by the layered architecture is significant. Let us call the ratio between the wiring complexity of a layered network and the wiring complexity of a single-layer network, the **complexity ratio**.

Fact 7. (a) For the network of Figure 17 ($P = 2$)

$$\text{Complexity Ratio} = \frac{2}{3}. \quad (110)$$

(b) For the network of Figure 19 ($P = 3$)

$$\text{Complexity Ratio} = \frac{3}{11}. \quad (111)$$

6. PHYSIOLOGICAL FACTS

This section describes how the lower vertebrate retina naturally solves an early vision problem utilizing architecture similar to those proposed in the previous sections. In particular, the SCE filter described in Section 4 has been inspired by several physiological facts described below. In the retina, especially that of lower vertebrates, neurons of a homogeneous type are occasionally coupled by electrical synapses to constitute a laminal structure, syncytium. Accordingly, several different syncytia form a multilayered structure and interact through local electrical or chemical synapses (Yagi, 1986; Yagi, Funahashi, & Ariki, 1989). Figure 23 shows a double-layered neural network consisting of a photoreceptor (PH) syncytium and a horizontal cell (HC) syncytium. Previous physiological studies have shown that in several animal species, PHs are coupled together by electrical synapses as well as HCs. The conductance of electrical synapses is symbolically represented by g_{s1} and g_{s2} for PH and HC, respectively.

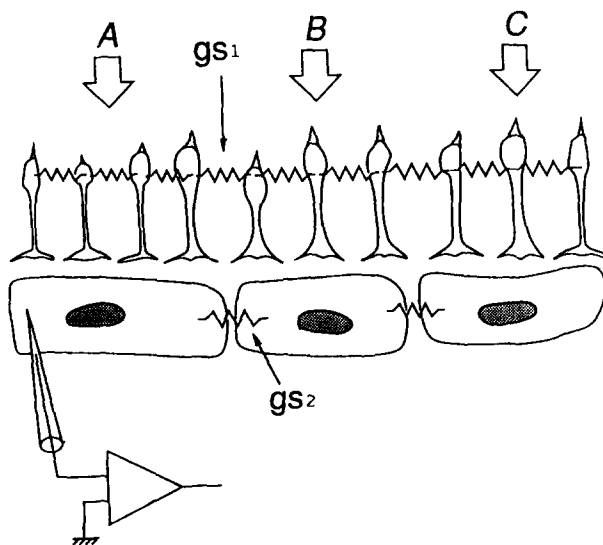


FIGURE 23. Schematic drawing of neural network consisting of photoreceptor and horizontal cell syncytia in the lower vertebrate retina. It is half morphological while half symbolic.

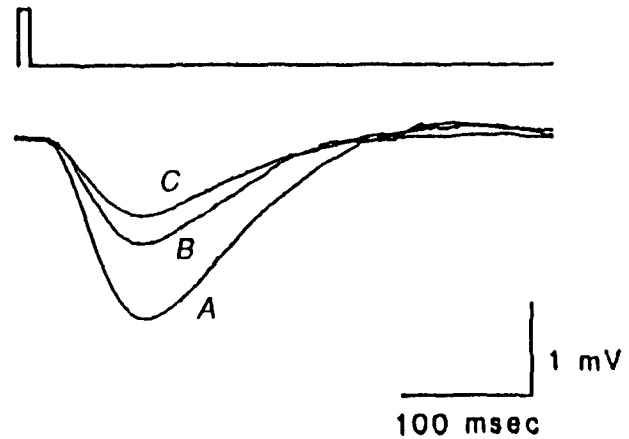


FIGURE 24. Measured horizontal cell response to a slit of light.

Therefore, this picture is half morphological and half symbolic. A piece of evidence demonstrating electrical coupling between HCs was obtained by intracellular recordings. As shown in Figure 24, the HC was penetrated by a microelectrode (indicated by the thin triangle) which is connected to the operational amplifier. The light-evoked response was obtained from a carp retina. Figure 24 shows superimposed responses to a flash of slit which was displaced by a 0.2 millimeter step from the recording site as illustrated by A, B and C in Figure 23. The response amplitude decreased as the distance between the slit and the recording site was increased, indicating that HCs are coupled through the electrical synapse. Similar observations have been made for PHs (Lamb & Simon, 1976; Schwartz, 1976).

Figure 15, discussed earlier, is in fact a model proposed by one of the authors based upon various measurements and considerations (Yagi, 1986; Yagi et al., 1989). Thus, one may think that the first layer of Figure 15 represents a PH syncytium and the second represents an HC syncytium. From previous physiological experiments made on lower vertebrate retina, $1/g_{m1}$ (the membrane resistance of PH) and $1/g_{m2}$ (the membrane resistance of HC) were estimated to be $1 \text{ G}\Omega$. $1/g_{s1}$ (the electrical synaptic resistance of PH) and $1/g_{s2}$ (the electrical synaptic resistance of HC) were $30 \text{ M}\Omega$ and $5 \text{ M}\Omega$, respectively. T_1 corresponds to the coefficient of chemical synaptic input from PH to HC and was estimated to be 1 nS . The only difference between Figure 15 and Figure 10 is the presence of T_2 in Figure 15, which is the feedback from the second layer to the first layer. This is known as a feedback synapse from HC to PH (Baylor, Fuortes, & O'Bryan, 1971). T_2 was estimated to be -1 nS (Ariki, Yagi, & Funahashi, 1990). Also T_2 is known to be negative while T_1 is known to be positive. It follows from Fact 3 that this network is spatially stable (see eqn (85)).

The following fact tries to interpret the information

processing mechanism of the lower vertebrate retina in the framework of the regularization theory. Even though a lower vertebrate retina is far from being as crisp as Figure 15, one can see the role of PH and HC in visual information processing in an interesting way:

Fact 8. In early vision of lower vertebrate retina, the following interpretation is possible:

1. Given the u_k , horizontal cells perform the second order regularization with

$$\lambda_2 = \frac{g_{s1}g_{s2}}{g_{m1}g_{m2} - T_1T_2} = \frac{4}{3} \times 10^4,$$

$$\lambda_1 = \frac{g_{m1}g_{s2} + g_{m2}g_{s1}}{g_{m1}g_{m2} - T_1T_2} = \frac{14}{3} \times 10^2, \quad (112)$$

$$d_k = \frac{T_1}{g_{m1}g_{m2} - T_1T_2} u_k = 0.5 \times 10^9 u_k \quad (113)$$

and hence,

$$\frac{\lambda_1}{\lambda_2} = \frac{14}{4} \times 10^{-2} = 0.035. \quad (114)$$

2. Photoreceptors perform the first order regularization with

$$\lambda_1 = \frac{g_{s1}}{g_{m1}} = \frac{1000}{30} = 33.3,$$

$$d_k = \frac{1}{g_{m1}} (u_k + T_2 v_k^2) = 10^9 \times (u_k - 10^{-9} v_k^2) \quad (115)$$

simultaneously.

Figure 25 shows the response x_k , which corresponds to the bipolar cell in the retina based on the physiological data where

$$u_k = \begin{cases} 100 \text{ pA} & 99 \leq k \leq 101 \\ 0 & \text{otherwise.} \end{cases} \quad (116)$$

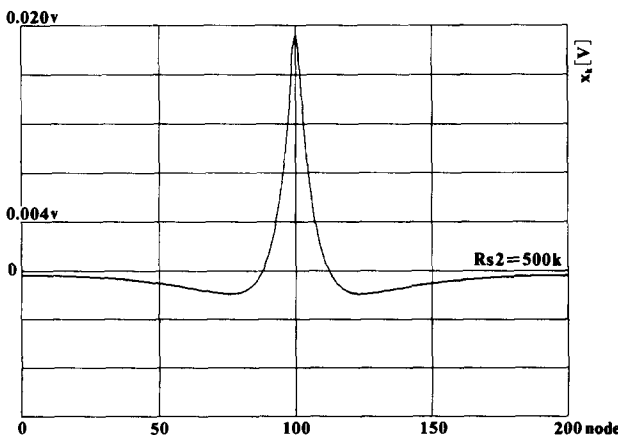


FIGURE 25. Simulated response with the physiological data.

Since $T_2 < 0$, one sees that $d_k = (u_k - |T_2|v_k^2)/g_{m1}$, which means that the first layer performs the first order regularization given the original data u_k minus the “local average” $|T_2|v_k^2$ which is quite reasonable to reduce the dynamic range. The multilayered architecture given in Figure 5(a) is a natural generalization (except for the feedback synapse) of the network consisting of PH and HC syncytia. In fact, the retina is known to have multilaminar structure consisting of several neural syncytia.

7. CONCLUSIONS

Layered architecture was proposed for solving a class of regularization problems in image processing. One motivation came from one of the authors’ experiences with the chip implementation of a second order regularization filter, where the architecture demands negative conductance and wiring between every pair of second nearest nodes in addition to the immediate neighbor wiring. The negative conductance gives rise to stability problems whereas the wiring complexity makes it difficult to layout the mask pattern of the chip. The layered architecture proposed in this paper is free from these stability problems because there is no negative conductance. The only active elements are voltage controlled current sources which are simple and popular in any circuit design. The architecture proposed in this paper demands only wiring between nearest nodes. It was shown that our discrete formulation is suited for the two-dimensional problems on a hexagonal array.

An attempt was made to quantify the wiring complexity of a network. It was shown that the layered architecture proposed significantly reduces the wiring complexity compared with single-layer architecture.

By specializing the number of layers to be two, the SCE filter was proposed. The filter enhances contrasts of input image as well as smoothing out noise. It was pointed out that voltage controlled current sources play several significant roles in accomplishing the filtering operation.

Since the processing (computation) is done by the dynamics induced by the parasitic capacitors of MOS transistors and since the processed image is given as the node voltage distribution at the stable limit point, the filter is extremely fast, with orders of magnitude faster than a digital signal processor. This naturally indicates applicability to smart sensing, i.e., to the simultaneous accomplishment of sensing and processing. This chip implementation has been completed and the chip is fully functional. The experimental results will be reported elsewhere.

It was explained how the layered architecture was inspired by the physiological findings on lower vertebrate retina obtained by one of the authors.

Possible future projects to pursue include:

1. Incorporation of other interesting physiological findings into image processing filters, e.g., an adaptation mechanism.
2. Studies of $N \geq 3$ regularization filters. A third order regularization is briefly discussed in Liu and Harris (1989).

REFERENCES

- Ariki, F., Yagi, T., & Funahashi, Y. (1990). Spatio-temporal responses of the dual layer neural network in retina. *Proceedings of the 5th Annual Symposium on Biological and Physiological Engineering*, 9–12.
- Baylor, D. A., Fuortes, M. G. F., & O'Bryan, P. M. (1971). Receptive field of single cones in the retina of the turtle. *Journal of Physiology*, **214**, 256–294.
- Clark, J. (1989). Authenticating edges produced by zero-crossing algorithms. *IEEE Transactions on PAMI*, **11**, 43–57.
- Dudgeon, D., & Mersereau, R. (1984). *Multidimensional signal processing*. Englewood Cliffs, NJ: Prentice Hall.
- Grimson, W. E. L. (1981). *From images to surfaces*. Cambridge, MA: MIT Press.
- Gruss, A., Carley, L. R., & Kanade, T. (1991). Integrated sensor and range-finding analog signal processor. *IEEE Journal of Solid-State Circuits*, **26**(3), 184–191.
- Harris, J. (1986). *The coupled depth/slope approach of surface reconstruction*. Master's Thesis, Massachusetts Institute of Technology, Cambridge, MA.
- Harris, J. (1988). An analog VLSI chip for thin-plate surface interpolation. *IEEE Conference on Neural Information Processing Systems-Natural and Synthetic*, **1**, 687–694.
- Harris, J., Koch, C., Luo, J., & Wyatt, J., Jr. (1989). Resistive fuses: Analog hardware for detecting discontinuities in early vision. In M. Mahowald & C. Mead (Eds.), *Analog VLSI implementation of neural systems* (pp. 27–56). Norwell, MA: Kluwer Academic.
- Hutchinson, J., Koch, C., Luo, J., & Mead, C. (1988). Computing motion using analog and binary resistive network. *IEEE Computer*, **21**, 52–63.
- Kobayashi, H., Matsumoto, T., Yagi, T., & Shimmi, T. (1991). A layered architecture for regularization vision chips. *Proceedings of the IJCNN 91, Singapore*, **2**, 1007–1020.
- Kobayashi, H., White, J. L., & Abidi, A. A. (1990). An analog CMOS network for Gaussian convolution with embedded image sensing. *ISSCC Digest of Technical Papers*, San Francisco, 216–217.
- Kobayashi, H., White, J. L., & Abidi, A. A. (1991). An active resistor network for Gaussian filtering of images. *IEEE Journal of Solid-State Circuits*, **26**(5), 738–748.
- Lamb, T. D., & Simon, E. J. (1976). The relation between intercellular coupling and electrical noise in turtle photoreceptors. *Journal of Physiology*, **263**, 257–286.
- Liu, S. C., & Harris, J. (1989). Generalized smoothing networks in early vision. *Proceedings of the IEEE Conference on Computer Vision and Pattern Recognition*, 184–191.
- MacKay, D. J. C. (1991). Bayesian methods for adaptive models. *Ph.D. Thesis*, Caltech, Pasadena, CA.
- Mathur, B., Lin, S. C., & Wang, H. T. (1990). Analog neural networks for focal-plane image processing. *SPIE*.
- Matsumoto, T. (1976). On the dynamics of electrical networks. *Journal of Differential Equations*, **32**(1), 179–196.
- Matsumoto, T., Kobayashi, H., & Togawa, Y. (1991). Stability of image processing neuro chips: Spatial and temporal. *Proceedings of the IJCNN 91, Seattle, WA*, **II**, 283–295.
- Matsumoto, T., Kobayashi, H., & Togawa, Y. (1992). Spatial versus temporal stability issues in image processing neuro chips. *IEEE Transactions on Neural Networks*, **3**(4), 540–569.
- Mead, C. (1989). *Analog VLSI and neural systems*. Reading, MA: Addison-Wesley.
- Mead, C., & Mahowald, M. (1988). A silicon model of early visual processing. *Neural Networks*, **1**(1), 91–97.
- Poggio, T., Torre, V., & Koch, C. (1985, Sept.). Computational vision and regularization theory. *Nature*, **317**, 314–319.
- Poggio, T., Voorhees, H., & Yuille, A. (1985). A regularized solution to edge detection. *MIT AI Laboratory Memo 833*, Cambridge, MA.
- Schwartz, E. A. (1976). Electrical properties of the rod syncytium in the retina of the turtle. *Journal of Physiology*, **257**, 379–406.
- Suter, D. (1991). Generalization of the Harris “coupled depth-slope” analog visual reconstruction network. *Proceedings of the IJCNN 91, Seattle, WA*, **I**, 729–739.
- Terzopoulos, D. (1984). Multiresolution computation of visible-surface representations. *Ph.D. Thesis*, Massachusetts Institute of Technology, Cambridge, MA.
- Tikhonov, A. N. (1963a). Solution of incorrectly formulated problems and the regularization method. *Soviet Mathematical Doklady*, **4**, 1035–1038.
- Tikhonov, A. N. (1963b). Regularization of incorrectly posed problems. *Soviet Mathematical Doklady*, **4**, 1624–1627.
- Tikhonov, A. N. (1965). Nonlinear equations of the first kind. *Soviet Mathematical Doklady*, **6**, 559–562.
- Whaba, G. (1987). Three topics in ill-posed problems. In H. W. Engl & C. W. Groetsch (Eds.), *Inverse and ill-posed problems* (pp. 37–51). New York: Academic Press.
- Yagi, T. (1986). Interaction between the soma and the axon terminal of retinal horizontal cells. *Cyprinus Carpio. Journal of Physiology*, **375**, 121–135.
- Yagi, T., Funahashi, Y., & Ariki, F. (1989). Dynamic model of dual neural network for vertebrate retina. *Proceedings of the IJCNN*, **1**, 787–789.
- Yagi, T., & Kaneko, A. (1987). Membrane properties and signal conduction of the horizontal cell syncytium of teleost retina. *Neuroscience Research Supplement*, **6**, 119–132.
- Yasuda, M., Yamaguchi, Y., Fukushima, K., & Nagata, S. (1971). An electronic model of visual receptive fields. *Transactions of the IECE*, **54-C**, 514–521.